Optoelectronic Metadevices

Son Tung Ha,[1#] Qitong Li,[2#] Joel K. W. Yang,[3] Hilmi Volkan Demir,[4,5], Mark L. Brongersma,[2*] Arseniy I. Kuznetsov,[1*]

[1]Institute of Materials Research and Engineering (IMRE), Agency for Science, Technology and Research (A*STAR), 2 Fusionopolis Way #08-03, 138634, Singapore.

[2]Geballe Laboratory for Advanced Materials, Stanford University, Stanford CA 94305, USA.

[3]Engineering Product Development, Singapore University of Technology and Design, 8 Somapah Road, Singapore 487372, Singapore.

[4]LUMINOUS! Center of Excellence for Semiconductor Lighting and Displays, The Photonics Institute, School of Electrical and Electronic Engineering, School of Physical and Mathematical Sciences, School of Materials Science and Engineering, Nanyang Technological University, 639798, Singapore.

[5]UNAM—Institute of Materials Science and Nanotechnology, The National Nanotechnology Research Center, Department of Electrical and Electronics Engineering, Department of Physics, Bilkent University, Bilkent, Ankara, 06800, Turkey.

*Corresponding authors. Email: brongersma@stanford.edu (M.L.B) and arseniy_kuznetsov@imre.a-star.edu.sg (A.I.K)

[#]These authors equally contributed to this work

Abstract: Metasurfaces have introduced new opportunities in photonic design by offering unprecedented, nanoscale control over optical wavefronts. These artificially structured layers have largely been used to passively manipulate the flow of light by controlling its phase, amplitude, and polarization. However, they can also dynamically modulate these quantities and manipulate fundamental light absorption and emission processes. These valuable traits can significantly extend their application domain to chipscale optoelectronics and conceptually-new optical sources, displays, spatial light modulators, photodetectors, solar cells, and imaging systems. New opportunities and challenges have also emerged in the materials and device integration with existing technologies. This review aims to consolidate the current research landscape and provide perspectives on metasurface capabilities specific to optoelectronic devices, giving new direction to future research and development efforts in academia and industry.

Metasurfaces are planar optical elements comprised of dense arrays of subwavelength nanostructures. Their desirable formfactor and ability to deliver a myriad of optical functions make them very attractive for a wide range technologies. Thus far, they have primarily been used to control the flow of light by capitalizing on the light scattering properties of the nanostructures. Here, their function is to passively transform one optical wavefront into another. However, there is an equally large opportunity to integrate metasurfaces directly into optoelectronic devices to control the emission, modulation/manipulation and detection of light. For example, metasurfaces can be integrated with light sources to realize large enhancements in radiative decay rates (i.e. Purcell effect) or to achieve new ways of dynamically controlling the angular and polarization properties of emitted light fields by e.g. patterning nanoscale electrodes. By merging nanoelectronics and metasurface technology, it is possible to create active metasurfaces capable of dynamically shaping optical wavefronts and to deliver new designs for beam steering (e.g. for Light Detection and Ranging (LiDAR)) and optical sensing platforms. Metasurfaces can also be embedded into photodetectors to realize never-before-seen functionalities. Here, one can engineer optical fields inside metasurfaces to enhance absorption efficiency for specific light waves of interest and open the door to new photodetectors, solar cells and computational imaging functions.

Integrating metasurface concepts into optoelectronic devices is an essential step towards the commercialization of this technology. While the promise of densely integrating planar electronics with planar metasurfaces into ultra-compact device platforms is evident, it faces a number of challenges towards the practical implementation. These challenges include scalable fabrication techniques, material compatibility, the need for careful co-design of the optics and electronics, and system-level integration. Addressing these issues is crucial to unleash the full potential of metasurfaces and ensure their widespread adoption.

In this paper, we will give an overview of the state-of-the-art metasurface-based optoelectronic devices, highlighting key achievements, underlying principles, and technological challenges. We also discuss various strategies employed for metasurface fabrication, materials selection, co-design with electronics, and device integration while also exploring potential avenues for future research and development. By consolidating the existing knowledge and identifying the current obstacles, this review paper aims to provide researchers, engineers, and industry professionals with a roadmap towards successful commercialization of integrated metasurface technologies.

Co-design opportunities in nanoscale optoelectronic devices

The scaling of optoelectronic devices has come with many important benefits. Most notably, it has brought significant opportunities to reduce the power consumption of information processing and communication systems. Such systems are now consuming approximately 10% of the worldwide electricity production. The rapid developments in artificial intelligence and machine learning are projecting even higher energy requirements with a non-sustainable impact on greenhouse gas emissions (*1*–*3*). At the nanoscale, a number of beneficial physical effects naturally become available, including quantum mechanical effects and optical resonances that can deliver extreme

light-matter interaction (*4*, *5*). By judiciously structuring devices to capitalize on these effects, it is possible to gain dramatically improved control over the flow of charge and light to create new functionalities and achieve reductions in power consumption that go well beyond those expected from basic scaling rules.

The fabrication tools that have enabled the scaling in the semiconductor industry can also create high-performance optoelectronic devices and circuits in which semiconductors, dielectrics, and metals are interwoven at the nanoscale. Their assembly does not simply follow the same design rules as larger-scale optoelectronic systems and new design concepts can be harnessed to effectively leverage the strengths of each constituent and to capitalize on the benefits of dense, chip-scale integration. To illustrate these points, we analyze a number of nanostructured devices for light emission, modulation, and photodetection and emphasize opportunities that can enable radically improved system architectures that combine electronics and photonics together in a seamless, highly-integrated fashion. Figure 1 shows the summary of the most important optoelectronics metadevices, their typical device configurations, materials and functionalities enabled by metasurfaces. Our examples highlight that in nanoscale optoelectronic systems, the exact boundaries between optical, electronic, mechanical, and thermal elements are often blurred and many components can perform multiple functions simultaneously. This is very different from current large-scale systems, including state-of-the-art miniaturized devices, such as smartphone cameras, where the optical elements (e.g. lenses and color filters for imaging), electronics (e.g. photodetection and image processing), mechanics (e.g. zoom and image stabilization systems), and thermal elements (e.g. cooling) are all easily identified and spatially separated.

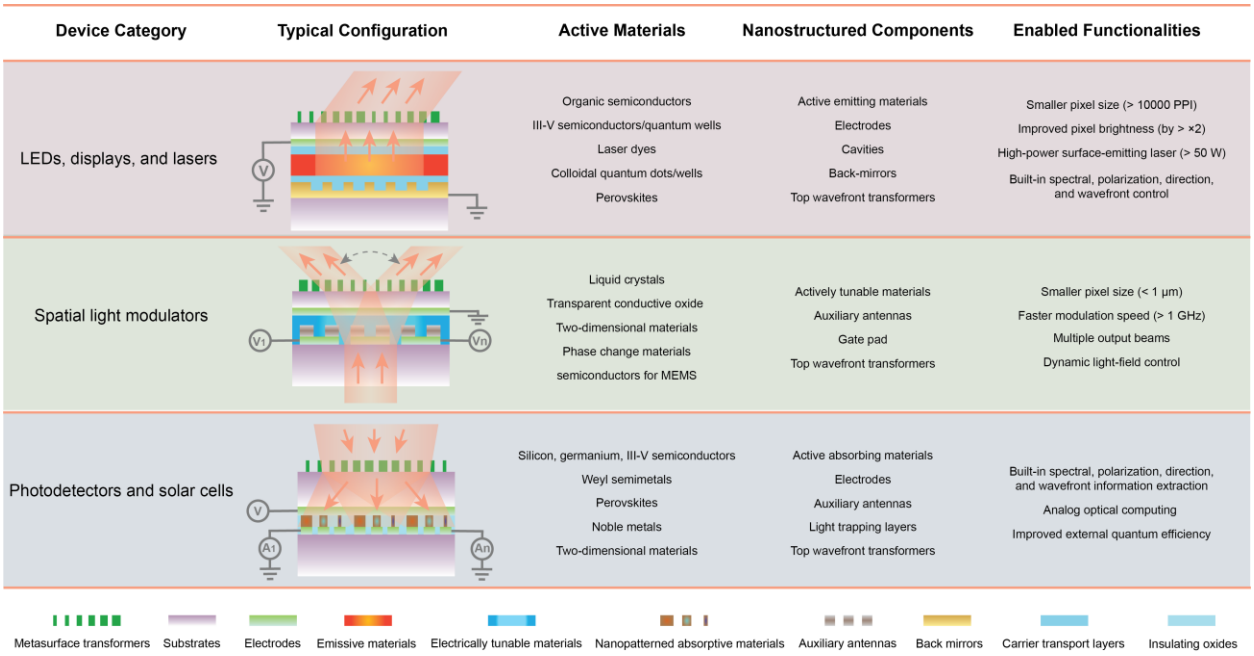

Fig. 1. Summary of different types of optoelectronic metadevices and enabled functionalities.

We will start by analyzing the multiple roles metallic structures can play in nanostructured optoelectronic devices. Metals serve an important role as high-conductivity electrodes for injecting/extracting charges and applying electric fields capable of modulating or tuning optical materials' properties. In addition to these electronic functions, nanopatterned metals can also be used in optical roles as light reflectors (*6, 7*), plasmonic resonators/waveguides (*8, 9*), or optical antennas (*10, 11*), capable of enhancing and controlling light-matter interaction. These optical functions need to be carefully optimized while not negatively impacting the electronic performance.

We first analyze the benefits of electronic and optical co-design for a simple, planar metallic electrode in an optoelectronic device that is patterned into a metasurface mirror. At first sight, it may seem that there is not much to optimize for a metallic mirror beyond its reflectance. However, in an optoelectronic device comprised of multiple thin layers, the reflection phase is at least as important as reflection amplitude since it governs the spatial location of the nodes and anti-nodes in the standing wave pattern in the electric field intensity (*7, 12, 13*). To achieve strong interaction with active absorber/modulation/emitter layers, it is critical to align the maxima in the electric field strength with the position of these layers. Unfortunately, often the use of high-conductivity, smooth metallic electrodes can cause issues as they produce a π phase reversal for reflected light waves creating a standing wave with an undesired, reduced light intensity near the reflective surface. To achieve strong light-matter interaction with a thin active layer, they need to be spaced approximately ¼ wavelength away from the metal and this may limit the charge injection or extraction (*14, 15*). This challenge can be circumvented by using a nanopatterned metamirror, as shown in Fig. 2A (*7*), whose reflection phase is tunable from that of a perfect *electric* mirror ($\varphi = \pi$) to a perfect *magnetic* mirror ($\varphi = 0$). This tunability in the reflection phase can also be exploited to ensure operation near a Fabry-Pérot resonance in a layered device. To benefit from such optical resonances, the roundtrip phase for light in the device needs to equal an integer number of 2π. Typically the roundtrip phase is tuned with the mirror spacing, but metamirrors can generate any desired reflection phase across the 0 - 2π range as shown in Fig. 2B (*7*). This leaves the mirror-spacing as a free parameter that can be optimized based on other considerations, e.g. electronic, fabrication ease, ideal materials choice, etc. Control over the anti-node positions and resonances can lead to notable enhancements in light absorption in thin photodetection and solar energy harvesting systems (*7*).

Besides engineering the reflection phase, nanopatterned metallic mirrors can also control the excitation and propagation of surface plasmon polaritons at the metal surface. Figure 2C shows the beneficial use of a metamirror in modulators to enhance light-matter interaction with an ultrathin active layer (*9*). In this work, a metal electrode can electrically modulate the intensity of a reflected light beam by electrically switching exciton resonances on and off in a two-dimensional (2D) semiconductor. Therefore, the performance of this modulator critically relies on the presence of a strong excitonic, material resonance. Excitons can offer extremely strong and high-speed optical modulation. However, such resonances severely weaken at room temperature where non-radiative decay dominates the radiative one. The application of a periodic nanopattern to the metal

surface brings the opportunity to grating couple incident, free-space photons to guided surface plasmons that notably enhance the light matter-interaction and also provide a favorable Purcell effect that boosts the radiative decay rate to such an extent that it can outpace the non-radiative decay at room temperature. Metallic strip-electrodes have also been utilized as plasmonic waveguides and as leads to apply fields in electro-optic modulators (*16*) or heating elements in thermo-optic modulators (*8*). In such designs, an outstanding overlap of the guided plasmon modes with the electrically-driven active medium is guaranteed.

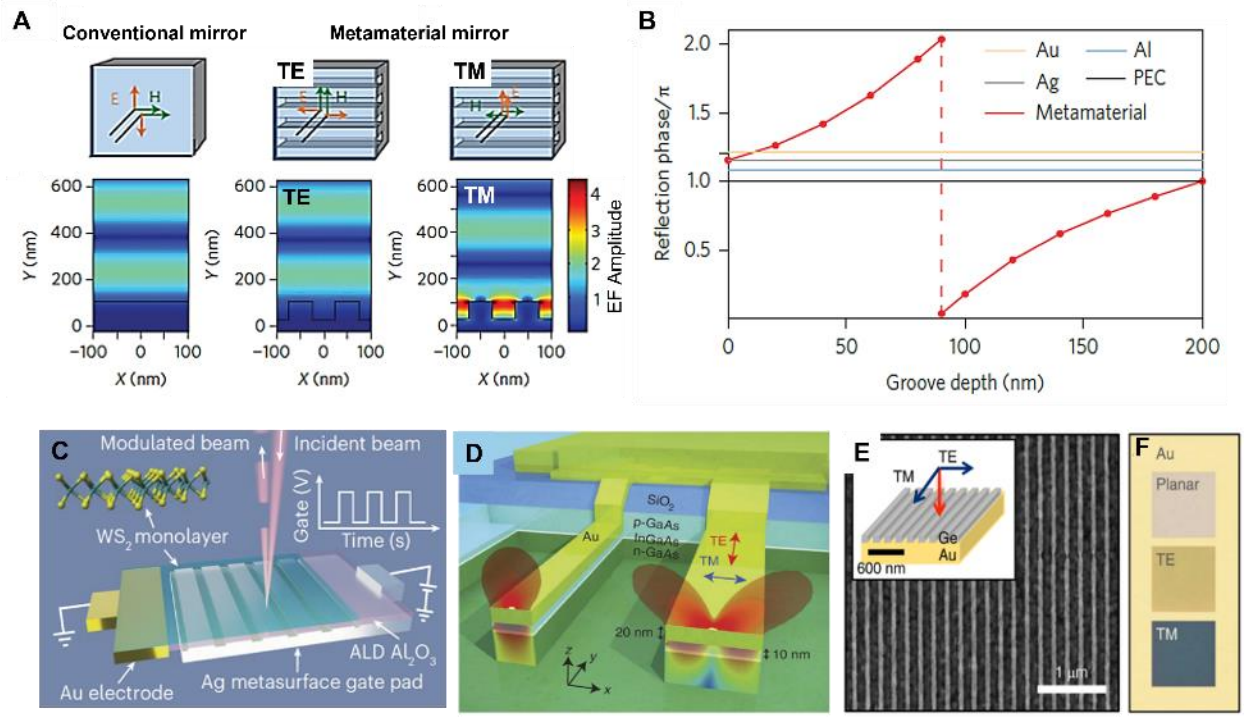

Fig. 2. Multiple roles of metallic and semiconductor nanostructures in optoelectronic devices. (**A**) Difference in the optical behaviour of a conventional mirror and a metamirror. In transverse electric (TE) polarization, the metamirror behaves as a conventional electric mirror that flips the electric field of an incident light wave on reflection, while for transverse magnetic (TM) polarization, it serves as a magnetic mirror capable of flipping the magnetic field (*7*). (**B**) Dependence of reflection phase from a metamirror on the metal groove depth (wavelength - 600 nm). The reflection phases for conventional metal reflectors are shown for comparison. PEC: perfect electrical conductor (*7*). (**C**) Schematic of a free-space optical modulator that capitalizes on the dynamically-tunable exciton resonances supported by the atomically-thin semiconductor WS_2 (*9*). A metal-oxide-semiconductor configuration is used to electrically gate the device. This can turn on and off the exciton resonances in the WS_2 and modulate the intensity of a reflected light beam. The nanopatterning of the metal electrode allows for the coupling to surface plasmons and an enhanced light-matter interaction. (**D**) Two Au electrodes of different widths can inject charge into a quantum well (QW) ridge. The electrodes also support distinct surface plasmon resonances that can be dipolar or quadrupolar in nature, depending on their width, as shown by the magnetic field amplitude maps within the semiconductor. When current is injected into the QW via the antenna-electrodes and the substrate, light is emitted with an angular emission pattern and polarization that is characteristic of the electrode dimensions (*11*). (**E**) Top-view scanning electron microscope (SEM) image of a fabricated metafilm with a 200-nm-period and 0.3-duty-cycle germanium (Ge) nanowires. The scale bar is 1 μm. Inset

shows a schematic of the measurements. (*17*). **(F)** White light reflection images taken from a thin 50 nm Ge film (top) and metafilms with 30-nm-wide beams under TE and TM illumination on an Au background.

Optical antennas can control the emission from quantum emitters by modifying the local density of optical states via the Purcell effect. This can deliver control over the decay rate of quantum emitters as well as the directionality and polarization of the light emission. However, their implementation in optoelectronic devices has been hampered by the need to precisely place emitters near an antenna and to efficiently excite them electrically. This requirement can be circumvented with the help of antenna-electrodes that facilitate simultaneous operation as electrodes for current injection and as antennas capable of optically manipulating the electroluminescence (*11*). Antenna-electrodes naturally deliver electrically-excited carriers to the vicinity of the antenna and maximize the optical coupling of the emission to a single, well-defined antenna mode (Fig. 2D).

Semiconductors also play vital roles in optoelectronic devices and there are unique opportunities for structuring them into metasurfaces as well. These materials can efficiently convert optical signals to electronic signals via the generation of photoexcited carriers, and vice versa through the recombination of electrically injected carriers. The prominent electro-optic and carrier effects in semiconductors can also be harnessed to modulate their coherent interaction with light. Simialr to metallic nanostructures, nanopatterned semiconductors also support strong optical resonances, termed Mie resonances (*5*), which endow them with improved and highly-engineerable light emission, modulation and absorption functions. On resonance, incident light waves can drive the bound charges in these highly-polarizable, high-index structures into oscillation. This produces intensified light fields inside and around the structure than can be used in devices. For example, in a semiconductor nanowire photodetector (*18*), the Mie resonances open up ways to spectrally engineer and enhance light absorption. These benefits can also be translated to judiciously nanopatterned semiconductor meta-layers. From the first systematic studies on structural colors on individual semiconductor nanostructures and metasurfaces (*19*), it became clear that the resonant behavior of the individual nanostructures could be encoded into metafilms assembled from these structures. By carefully choosing the sizes and spacings of nanostructures, near-unity light absorption can be achieved at one or more desired, target wavelengths (*17*). Figure 2E-F illustrate the impact of patterning a continuous germanium (Ge) film into a metafilm of densely-spaced nanowires. Figure 2F shows the normal-incidence reflection images taken for transverse magnetic (TM) polarized light with the electric field parallel to the length of the nanowires and for the orthogonal transverse electric (TE) polarization. Here, the anisotropic nature of the building blocks leads to different optical responses. Interestingly, the removal of about 2/3 of the Ge film gives rise to a greatly enhanced absorption under TM illumination as the weak Fabry-Perot resonance supported by the continuous Ge film is replaced by stronger Mie resonances of the nanowires.

The integration of resonant nanostructures into optoelectronic devices heralds a new era where the miniaturization of devices does not come at the cost of performance, and instead, opens up avenues for innovation in areas such as solar energy harvesting, imaging systems, and secure

communications. The potential impact and significance of metasurface-integrated devices lie in their ability to transform the landscape of technology, leading to smarter, more efficient, and highly adaptable optoelectronic applications. In the following sessions, we will discuss the current progress and challenges for each type of metadevices shown in Fig.1 in detail.

Light-emitting diodes and displays

In light-emitting diodes (LEDs), quantum emitters are electrically-driven to produce light by spontaneous emission. These devices are engineered with a desire to make the emission efficient, while also controlling different attributes of the generated light. However, the set of these attributes and the extent to which they can be controlled are usually limited. Typically, the peak emission wavelength and emission linewidth are determined by the choice of emitters. However, the available options are often limited to semiconductor epitaxial thin films, colloidal nanocrystals, and organic molecules/polymers. As a result, achieving precise desired emission characteristics may require compromises on emission efficiency and material's stability. For example, the spectral sharpness of spontaneous emission can be challenging to achieve due to its instrinsic homogenous broadening and inhomogeneous broadening due to the variation among contributing emitters. The tuning range of the peak emission without changing the optical output level can also be adversely limited. Similarly, the quantum efficiency of an emitter and performance of its resulting LED (external efficiency) might also be severely constrained. This translates to limited levels of optical brightness and, most of the time, a limited optical power output of a light-emitting device, after a certain point no matter how hard the device is driven. This may thus require the use of increased numbers of emitters (either a thicker film or a wider film area), bringing about other problems, including fabrication challenges and issues of uniformity and aging.

Another constraint of conventional LEDs is related to their radiation pattern, which is determined by the optical materials' properties. The extraction efficiency of the generated photons is therefore inherently limited by the dielectric environment and surface morphology of the LED. In most cases, the emission cone is wider than necessary, resulting in poor photon management and reducing the usable power of the generated light. Further patterning of the emitter film in pixelated LEDs to *e.g.* realize displays can introduce additional difficulties, especially for very high pixel densities across large areas. Moreover, in some applications where polarized light is needed, it is challenging to produce it with isotropic emitters (e.g., QDs) without additional optics. More complex functions, such as vortex beam generation or rapid emission modulation is not possible to achieve by solely manipulating the emitters.

Metasurfaces can be integrated into LEDs to transform the emitted light wavefront (*20–22*) or shape the emission of embedded emitters (*6, 23, 24*). These devices are termed 'meta-LEDs', where meta-optics concepts are applied as integral parts of the emitters and/or parts of the device structure (*25, 26*). Their impact can be truly transformative if they can substantially enhance the emission and extraction efficiencies and improve control over the angular and polarization properties of the

emitted light. Designers may use a single metasurface aimed at delivering one of these benefits, or adapt multiple structures to achieve multiple benefits in a single device.

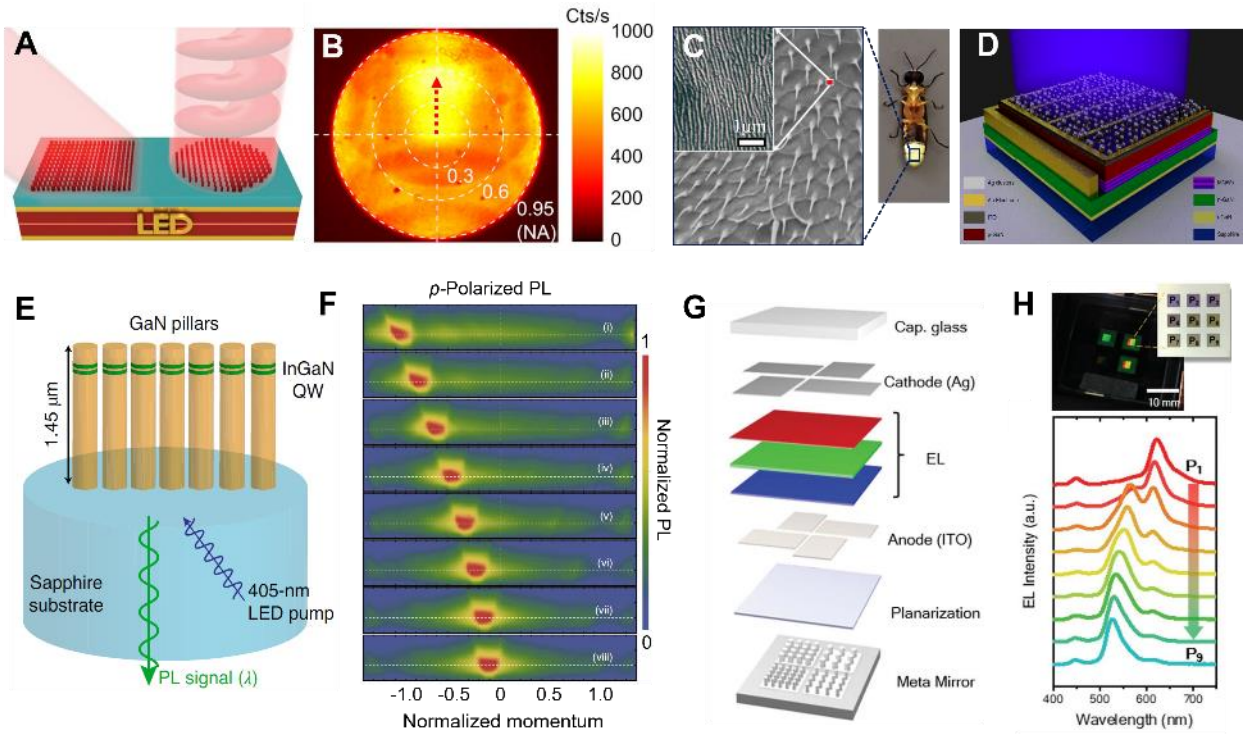

Fig. 3. Metasurface-based LED devices and displays. (**A**) Beam bending and vortex beam generation by integrating a metasurface onto a collimated LED device (*21*). (**B**) The back focal plane image of the photoluminescence (PL) from a GaP meta-LED showing the beam bending effect by the metasurface on top of the LED structure. PL was excited with a 488 nm continuous wave (cw) laser and collected using a microscope objective with numerical apature (NA) of 0.95 (*21*). (**C**) The SEM image of the microstructures on lantern cuticles of Pyrocoelia rufa firefly. The inset shows the microstructures with a higher magnification showing the disorder in both position and size of stripes (*22*). (**D**) Schematic (not to scale) of a GaN LED with a disordered metasurface patterned on top to enhance light extraction (*22*). (**E**) Illustration of a GaN nanopillar system with embedded InGaN multiple QWs (green) grown on a GaN base layer on a double-side polished sapphire substrate (*23*). (**F**) p-polarized PL as a function of wavelength (y axis, 520–580 nm) and normalized in-plane momentum ($k_{||}/k_0$; x axis) for the eight different GaN metasurfaces (*23*). (**G**) Cross-section of a meta-OLED with red, green and blue emitter layers. The different patterns created in the meta-mirror electrode control which colours benefit from a desirable Purcell effect and are effectively emitted from the device (*6*). (**H**) (Upper panel) Photo of a meta-OLED test cell that consists of four sections and is driven at 3 V. The inset shows an optical microscopy image of three-by-three metamirrors with different pitches (P1 to P9). (Lower panel) The electroluminescence from the device shown in (G) where the subwavelength period of the nanopattern is varied from 160 nm to 380 nm to achieve different emission colors (*6*).

For example, a metasurface can be patterned directly on the top or bottom surface of the device (i.e., contact layers) (*27*). In this configuration, the metasurface acts as a far-field wavefront transformer. Figure 3A shows the concept of integrating a metasurface with a collimated LED to manipulate its emission properties. The advantage of this concept is that the patterning of the metasurface does not affect the integrity of the LED structure and thus minimizes the device efficiency degradation. Using this concept, beam bending of gallium phosphide (GaP) LED emission was demonstrated (Fig. 3B) (*21*). Metasurfaces can also be used to enhance the emission extraction efficiency, especially when LEDs are made of high index materials such as III-V semiconductors. Figures 3C&D present a disordered metasurface concept inspired by nature to enhance the performance of a gallium nitride (GaN) LED (*22*). In addition to enhanced light scattering, disordered metasurfaces offer broadband optical response and introduce unique optical properties through multiple scattering effects. These structures have been extensively studied for various applications from light extraction to energy harvesting (*28, 29*).

Another approach to integrate metasurfaces into LEDs is by placing them in the near-field of the emitter layers. This involves defining a resonant nanostructure, such as a metasurface interlayer, directly above, below or within the emitter film. The metasurface can also be filled with emitters by either carefully placing them into the resonance 'hot spots' or by covering the entire structure with an emitter film (*23, 30*). Figure 3E shows an LED configuration where a nanopillar array is patterned into the active layer (i.e. multi quantum well). In this case, the GaN metasurface modifies the phase of the emitted light by leveraging the collective resonances of the nanopillars. This phase manipulation effectively alters the in-plane momentum of the emitted photons following the grating equation, redirecting them into specific angles, as shown in Fig. 3F. Recently, it was also demonstrated that patterned electrodes can control the Purcell effect in organic light-emitting diodes (meta-OLEDs, Fig. 3G, H) to deliver high spectral purity emission without the need for absorbing color filters at a record-high pixel density of ~10^4 pixels per inch (*6*). When incorporating metasurfaces into an emitter layer, the major challenge is achieving uniform charge injection to avoid issues such as current crowding, local heating, increased resistance, higher turn-on bias, voids, and short circuits which may degrade the device's performance.

The presented examples show that the integration of metasurfaces into LEDs offers significant advantages by improving performance and adding functionality. Metasurfaces allow precise control over light emission, enabling tailored spectral and angular properties. This leads to higher efficiency, color purity, and the integration of advanced optical functions such as beam shaping and polarization control.

LASERs

Light Amplification by Stimulated Emission of Radiation (LASER) devices play a crucial role in modern technologies, forming the foundation for various applications including medical surgeries, communication networks, manufacturing, and scientific research. Metasurface-based lasers can offer distinct advantages over traditional laser designs by precisely controlling the emission

properties such as beam profile, directionality and polarization. In addition, metasurfaces can facilitate ultrafast tuning of laser properties, which is crucial for applications requiring rapid response times, such as in optical switching and sensing technologies. This level of control and flexibility makes metasurface-based lasers incredibly versatile and efficient, marking a significant advancement in the laser technology.

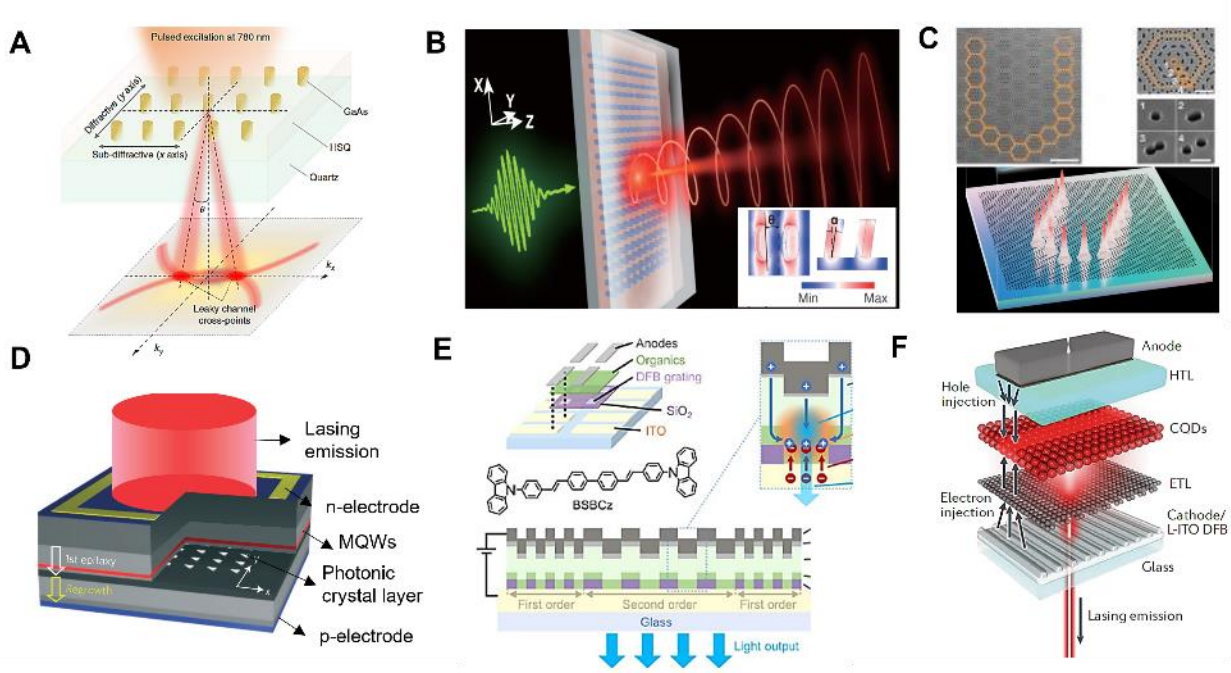

Fig. 4. Metasurface-based lasers. (**A**) Schematics of a GaAs nanopillar array on a fused silica substrate embedded in hydrogen silsesquioxane (HSQ) resist (i.e., spin-on-glass). Along the x-axis, the period is fixed at 300 nm (i.e., sub-diffractive) to support a symmetry-protected bound state in the continuum (BIC) mode at ~825 nm, while along the y-axis, the period P_y is set at 540 nm to create diffractive leaky channels for the directional emission of the laser. (*31*). (**B**) Schematic of chiral BIC metasurface made of TiO_2 that can produce chiral lasing with a maximum DOP of 0.98 when coupled with a gain medium such as 2-methyl-6-(4-dimethylaminostyryl)-4H pyran. The chiral BIC mode is formed by doubly breaking geometrical symmetry as shown in the insets (*32*). (**C**) (Upper panels) SEM images of the U-shaped Moiré nanolaser composed of 17 unit cells of a Moiré superlattice highlighted by orange hexagons. The Moiré superlattice is fabricated in a semiconductor membrane consisting of InGaAsP multiple QWs. Scale bar, 5 μm. (Lower panel) Schematic of a coherent, reconfigurable Moiré nanolaser array that emits U patterns with phase locking (*33*). (**D**) Schematic of the InGaAs-based photonic crystal surface-emitting laser (PCSEL) where the photonic crystal structure is created by patterning an air-hole array in a p-AlGaAs cladding layer. Arrows indicate the growth direction of the first epitaxial and regrowth structures (*34*). (**E**) Schematic representation of the organic laser diode (OLD) structure employing DFB cavity consisting of SiO_2 nanobeams with widths of 140 and 70 nm for second- and first-order gratings, respectively. Bright, narrow emission and threshold-like behavior were observed under pulse operation at 50V (*35*). (**F**) A proposed quantum dot laser diode (QLD) architecture, which comprises a p-i-n structure assembled on top of a DFB cavity integrated into a lower indium tin oxide (L-ITO) electrode. HTL: Hole transport layer; ETL: Electron transport layer. CQDs: Colloidal quantum dots (*36*).

The concept of nanopatterned lasers has first been explored in photonic crystals, which were successfully applied to obtain high quality (*Q*) factor laser cavities. Both photonic crystal- and metasurface-based lasers exploit the nanoscale periodic structures to control light propagation and amplification. While the traditional photonic crystal approach relies on the photonic bandgap of periodic structures, metasurfaces offer greater control by using collective resonances of meta-atoms in an array. This allows for additional flexibility in engineering both the *Q*-factor and the emission properties of the laser. For instance, plasmonic metasurfaces, despite their intrinsic Ohmic losses, have been effectively used in optically pumped lasing devices thanks to their high-*Q* band edge modes (*37*). These narrow resonances, referred to as surface lattice resonances, arise from the diffractive coupling of localized surface plasmon resonances (LSPRs) of individual nanoparticles via evanescent diffraction orders, known as Rayleigh anomalies (RAs). The suppression of the radiative losses and associated high *Q*-factors come from the strong coupling between the RAs and LSPRs, which can be optimized by controlling their detuning. Recently, a way to dramatically reduce loss in plasmonic arrays by utilizing non-local surface plasmon polaritons (SPP) was proposed (*38*). The transition from local to non-local mode by coupling with diffraction order helps suppressing radiative losses and achieve high-*Q*. The rise of dielectric resonant nanostructures in recent years with their rich electric and magnetic resonant responses reignites the interest in creating the finest optical resonators for lasers with full control over directionality, polarization and mode profile. Recently, photonic concepts such as the bound state in the continuum (BIC) have been extensively studied and utilized for lasing devices. Figure 4A shows a directional surface-emitting laser concept by using a periodic array of GaAs nanopillars that support vertical electric dipole resonance (*31*). When these identical dipoles oscillate in phase, the destructive interference leads to the formation of symmetry-protected BIC at the Γ point (i.e., vertical direction). Fundamentally, BICs in periodic photonic lattices are singularities of polarization vortices in the far-field radiation, with the BICs located at the center of the vortex (Γ point in this case). Topological charge of a BIC mode can be determined by the winding number of the polarization vector around the singularity. Lasing emission can not couple to the singularity point due to the dark mode nature of BIC but rather to a quasi-BIC mode at an oblique angle. By controlling the radiative loss of the quasi-BIC mode via opening leaky diffraction channels, directional lasing can be achieved at desired angles. BICs can also happen at an off-gamma angle (so-called, accidental BIC or Friedwich-Wigner BIC) when geometrical parameters of the photonic structures are carefully tuned (*39, 40*). By merging multiple BICs with different topological charges, an even more efficient optical cavity, namely a superBIC, can be created, which has been proven to further lower the lasing threshold (*41, 42*). Another way to improve the *Q*-factor of BIC cavities with a finite-size array is to use photonic crystal structures with suitable bandgaps at the array boundaries. By using this approach, a *Q*-factor of $>10^6$ in a BIC cavity with an array size of only ~10×10 μm^2 has been experimentally demonstrated (*43*). The difference between BIC lasers and traditional surface-emitting lasers (e.g., Vertical Cavity Surface Emitting Lasers, VCSEL) is that the emitted photons constitute a polarization vortex due to the non-zero topological charge nature of BICs. These polarization states are intrinsically associated with the symmetry of the system. By using a two-beam pumping configuration, ultrafast all-optical

switching of a BIC laser mode was achieved with a record switching speed and power (*44*). Breaking the symmetry of the nanostructures can also be used to generate lasing emission with circular polarization. Figure 4B shows the TiO_2 nanopillars, specially etched to create tilted structures, which breaks mirror symmetry in the vertical direction. Using this structure, chiral lasing emission was demonstrated with a near-unity degree of polarization (DOP) (*32*). A similar approach was used to demonstrate a chiral metasurface with a high *Q*-factor and circular dichroism by using a TiO_2 slanted hole structure (*45*). In this case, by breaking the symmetry of the nanostructure twice (i.e., in-plane and out-of-plane symmetries), the topological charge of the symmetry-protected BIC can be split and fine-tuned to maximize the purity of the circular polarization. Moiré effects have also been used to demonstrate reconfigurable nanolaser arrays, as shown in Fig. 4C (*33*). The strong localization of the mode within a single unit cell of the Moiré superlattice is induced by a flatband resonance, which is formed when the Moiré twisted angle is carefully tuned. Using this concept and structured pumping technique, various lasing patterns were obtained with high spatial and spectral coherence (*33*). Leveraging the same concept of twisted lattices, the same group has also demonstrated a singular dielectric nanolaser with an ultrasmall mode volume of only ~0.0005 λ^3 (*46*). Other concepts such as Dirac singularity (*47, 48*), supersymmetry, topological insulator (*49–51*), and parity-time symmetry (*52*) have also been employed to design new optical cavities for lasers.

While numerous concepts for the use of resonance nanostructures in lasers have been suggested, their integration into electrically pumped devices remains a significant challenge. The reason is that the electrical device requirements have not been considered during the photonic design, including the material choice (e.g., conduction band alignment, hole and electron mobility), device architecture (e.g., electrodes, charge injection pathway), and thermal management. In this regard, an optimal photonic design that works well in an optically pumped laser configuration does not necessarily result in a good electrically pumped laser device. To date, there are three main electrically-pumped laser device platforms that have been successfully integrated with resonant nanostructures. The first and most efficient one is based on epitaxially-grown III-V semiconductors. Here, a resonant nanostructure can be patterned in between epitaxial growth cycles of different device layers as shown in Fig. 4D (*34*). Using this device concept (termed a photonic crystal surface-emitting laser – PCSEL), a watt-class laser device (*34*), and most recently, continuous wave single mode laser (*53*) were demonstrated. The successful integration of resonant nanostructures near the gain medium of PCSEL devices became possible with a novel regrowth strategy and careful design of photonic nanostructures to ensure an uncompromised electrical performance. The second, long-sought-after lasing platform is based on organic light emitting diodes (OLED) that offer tremendous versatility in their fabrication and benefit from a wide selection of emitting materials to deliver different lasing wavelengths. Figure 4E shows an organic laser diode (OLD) structure having a nanopatterned distributed feedback (DFB) cavity that has been reported to achieve lasing with electrical injection (*35*). The results show that it is possible to achieve high device performance after integrating it with an electrically-passive nanostructure made of SiO_2. This opens up the possibility to incorporate resonant nanostructures with novel functionalities into such lasing device structures. The third device platform is a quantum dot (QD)

laser diode (QLD) as shown in Fig. 4F (*36*). QDs made of II-VI semiconductors such as CdSe/CdS can offer several advantages over organic molecules as emitting materials for lasing. They exhibit higher photostability, tunable emission wavelengths through size and composition control, and narrower emission spectra, leading to better lasing performance.

Each device platform has its own challenges when it comes to the integration of resonant nanostructures to form efficient optical cavities without sacrificing electrical performance. For instance, the requirement in lattice mismatch for epitaxial growth in the III-V platform prohibits the use of foreign materials for nanostructures. Etching the whole stack of devices to form resonant nanostructures often results in poor electrical performance. For OLD and QLD, the main issue lies in the low charge injection tolerance of the materials which is usually below the high current density required for lasing. In addition, due to the thin-film nature of the devices, any defect due to the integration of resonant nanostructures may result in current crowding and material breakdown. Another important aspect of lasing devices is thermal management during their operation (i.e., at high current density). This is especially important for OLD and QLD where most of the materials constructing the lasers have low thermal conductivity. Addressing all these challenges alongside photonic design aspects is essential for successfully integrating photonic nanostructures into electrically-pumped laser devices.

The realization of resonant nanostructure-based laser devices with rich optical functionality will have a significant impact and applications in various fields such as sensing, optical communication, and quantum technology. Considering the recent progress in nanophotonic design, as mentioned earlier, along with innovative device architectures (*50, 54, 55*) and material advancement (*55, 56*), it is anticipated that the field will mature in the near future.

Optical modulators and switches

While static metasurfaces have already found their way into multiple optoelectronic applications, the possibility of imparting them with dynamically-tunable functionalities has always been a challenge in the metasurface community (*57–59*). Particularly, making each nanoantenna pixel in the metasurface independently tunable for either phase or amplitude modulation could help to achieve sub-wavelength dynamic control of optical wavefronts, not available within the current technologies. This can open widespread opportunities for applications of such tunable metasurfaces in two-dimensional (2D) and three-dimensional (3D) holographic projectors, augmented and virtual reality (AR/VR) devices, LiDAR for autonomous driving, and more (*60*). To achieve this ambitious goal, metasurfaces will have to be integrated together with electrical circuitry (i.e. Complementary Metal-Oxide-Semiconductor (CMOS) electrodes) to drive them at the individual pixel level.

The first studies of electrical switching of metasurfaces have mainly focused on different material platforms, which can provide sufficient tunability to achieve significant phase (~2π) or amplitude (~1) modulation. Liquid crystals (*61–63*), phase change materials (*64–68*), and semiconductors (*69–74*) are the most promising platforms from a practical device perspective, each having its own

advantages and disadvantages. Other switching mechanisms such as mechanical, thermo-optic, electro-optic, and electrochemical tuning have also been investigated and can be found *e.g.* in a recent detailed review (*75*).

Liquid crystals provide high refractive index changes, low switching voltages (i.e., a few Volts), low optical losses in the visible spectrum and long-term stability after multiple switching cycles. However, they suffer from relatively low switching speeds (>1ms) and crosstalk between the pixels (*61–63*). Phase change materials also can deliver a high refractive index change and can keep the changed state without the application of an extra voltage (i.e., nonvolatile switching) but suffer from higher switching voltages required to heat the material and fatigue effects at many switching cycles (*64–68*). Electrical gating of semiconductors can be very fast, allowing > GHz operation, but comes with undesirable light absorption and only achieves notable refractive index changes in very thin accumulation, depletion, or quantum-well layers (*69–72*). While there is currently no ideal switching mechanism that can satisfy all requirements at once, one can select a good material platform that is most suitable for a specific application. For example, AR/VR and holographic display applications can benefit from high diffraction-efficiencies in the visible spectrum and high cyclability offered by liquid crystals, while being tolerable to their relatively slow (>1ms) switching speed (*61, 76*). On the other hand, LiDAR devices and communication systems could benefit from the high switching speeds provided by gating semiconductors (*70*), while being less demanding to electrical tunability of the metasurface building blocks. Phase change materials could be most suitable for reconfigurable static displays or reconfigurable optics where constant cycling of the material is not required. In such applications the nonvolatile switching, which does not require constant voltage application, could be of great advantage to save energy between rare switching events (*67*).

Another important consideration is the smallest pixel pitch at which the metasurface can be switched without the unwanted crosstalk between neighboring pixels. From an application perspective, it is important to reach a pixel pitch significantly smaller than the existing technology can provide, e.g. a 3.74 µm pixel-pitch for liquid on silicon (LCOS) phase-only spatial light modulator (SLM) from Holoeye (*77*). For liquid crystal-based tunable metasurfaces, the individual pixel switching down to a pitch of ~1 µm has been demonstrated (Figure 5A-C) (*61, 63*). The diffraction efficiency of such devices reaches >40%, making it promising for a range of applications, including displays and laser projectors. Further pitch reduction in such tunable metasurfaces is possible but requires dealing with the crosstalk induced within the thin liquid crystal layer as well as the optical interaction between neighboring dielectric nanoantennas. Even smaller pitches of ~500 nm, down to the single nanoantenna level, have been demonstrated for plasmonic metasurfaces based on gating effects, but with a much lower efficiency of a few percent only (*71*). Potential applications of such metasurfaces to LiDAR technology have also been shown (Figure 5D-E) (*70*). For phase change materials, while switching of an individual nanowire and nanoantenna arrays have been demonstrated (*64–68*), individual switching of multiple pixels in a metasurface array has not yet been achieved. Here, a thermal crosstalk between the pixels related to the heat-induced switching mechanism should be taken into consideration. Individual pixel

control has also been shown e.g. in plasmonic metasurfaces switched by conducting polymers (*78–80*).

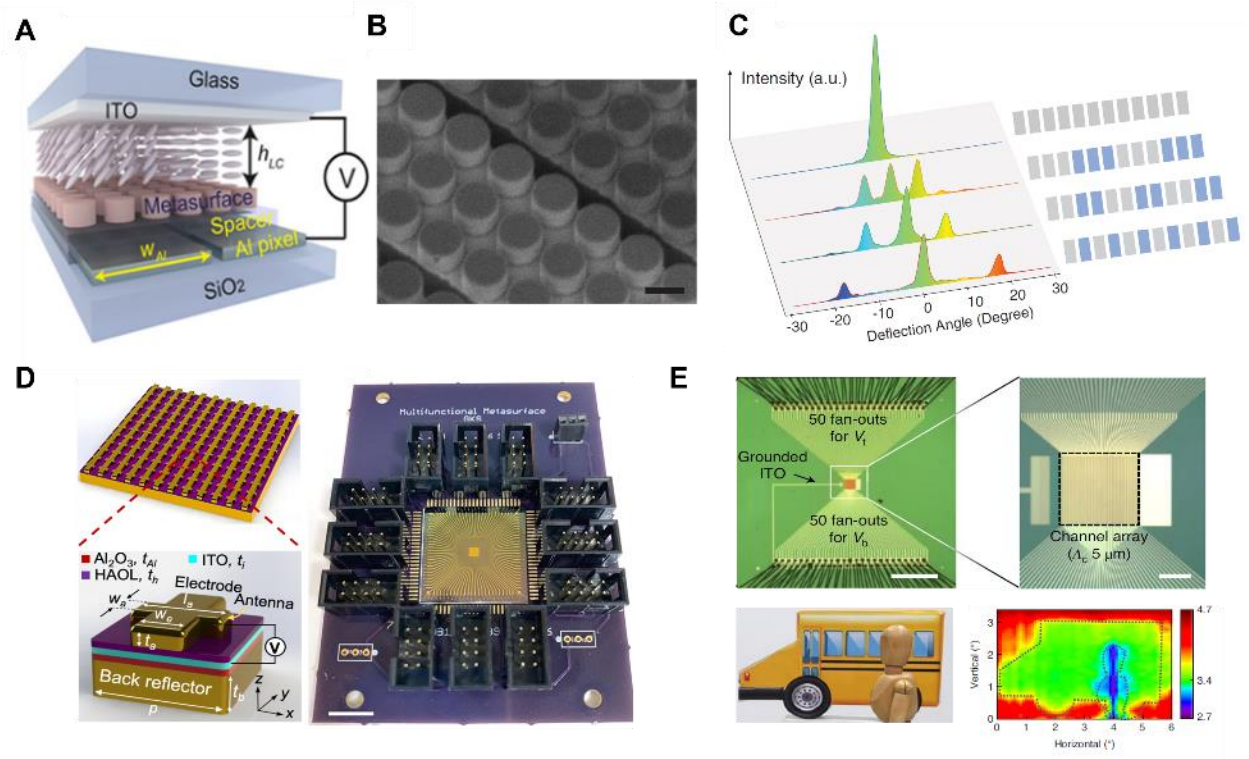

Fig. 5. Examples of tunable metasurface devices and their applications. (**A**) Schematic of a single-pixel tunable reflective metasurface device based on liquid crystals (*61*). (**B**) Zoom-in SEM image of 1-μm tunable metasurface pixels with integrated dielectric nanoantennas (*63*). (**C**) Tunable diffraction grating generated by a transmissive liquid-crystal-tunable metasurface with individual pixel control (*63*). The left side shows the experimentally measured diffraction intensities as a function of the deflection angle for different electrode-addressing configurations, shown on the corresponding right side. Gray patches represent grounded electrodes, and blue patches represent biased ones (at 8 V). a.u: arbitrary units. (**D**) (left) Schematic of a single-pixel tunable reflective plasmonic metasurface device based on the electrical gating effect. The device consists of an Au back-reflector, an Al_2O_3 dielectric layer, an ITO layer, and a hafnium oxide/aluminum oxide laminated (HAOL) gate dielectric followed by an Au fishbone nanoantenna. (right) Sample mounting circuit board to control the multifunctional metasurface with 96 individually addressable linear pixels. Scale bar is 10 mm (*71*). (**E**) (Top) Optical image of the active metasurface array located in the middle of the fan-outs with a size of 250 × 250 μm^2. For the dynamic wavefront manipulation, operating blocks with the period Λ_C of 5 μm were used. Scale bar is 100 μm. (Bottom) A model object for 3D imaging (left) and 3D depth image produced using the metasurface-based SLM (right), which demonstrates the feasibility of the use of the device as the core scanning component in a LiDAR system. The scan angle range, angle step size and resolution are 6° (H) × 4° (V), 0.2° (H) × 0.2° (V) and 31 × 21 = 651, respectively, where H and V denotes the horizontal and vertical axes, respectively (*70*).

The single-pixel tunable metasurface demonstrations mentioned above have only shown 1D arrays of switchable pixels able to produce active beam steering along a single direction. To unleash the full potential of tunable metasurface technologies, however, addressing a 2D array of pixels with individual pixel control is required. The first attempts to do it using conventional single-layer electrode fan-out could only produce small (10 × 10) arrays of 5.2 × 5.2 μm^2 pixels (*69*), which are far below of what commercial applications require. Transitioning to a larger number of pixels with much smaller sizes would require integration of metasurfaces on top of CMOS circuitry, which can apply different voltages to individual pixels using a control circuit containing transistors beneath each pixel. This, in turn, will impose additional limitations on the maximum voltage, which can be applied to each pixel without destroying the CMOS circuit. A recent presentation showed this kind of integration of a liquid crystal-tunable metasurface on top of a 480 × 640 array (VGA resolution) of 1.1 × 1.1 μm^2 CMOS pixels (*76*). With voltages changing in the range of 1-2V, the authors were able to demonstrate dynamic switching of individual pixels, opening the door to realizing 2D dynamic beam steering and tunable 2D holograms with a 100 Hz refresh rate. These results mark a significant improvement compared to the current state-of-the-art technologies available in industry, showing a strong potential of tunable metasurface devices for practical applications. Further developments in this field are necessary to facilitate commercialization of this technology. This would require simultaneously ensuring multiple factors including small-voltage switching, high diffraction efficiency, fast refresh rates (depending on the application), low power consumption, high uniformity of phase and amplitude modulation across large pixel arrays, and material compatibility with large-volume manufacturing platforms. These are largely associated with engineering and device optimization rather than fundamental issues.

Photodetectors, Spectrometers and Imaging Systems

The photodetectors found in commercial devices, such as imaging sensors, proximity sensors, and spectrometers, commonly rely on semiconductor p-n junctions, Schottky barriers, or the photoelectric effect to convert optical signals into electrical ones. They are well-suited to measure the light intensity, but all other information carried by the incident photons is typically lost in the photodection process. Beyond intensity, various properties of light, such as wavelength, phase, polarization, orbital angular momentum (OAM), propagation direction, spatial and temporal coherence remain challenging to detect directly with conventional photodetectors without introducing bulky optics. Metasurfaces offer a promising platform to enable the detection of this rich set of properties of light through compact integration of sub-wavelength meta-atoms with photodetection/imaging systems. With sophisticated design involving geometry, antenna layout, and suitable materials, recent demonstrations of these metasurface-integrated photodetectors (MIPDs) promise a new generation of photodetectors and imaging systems.

In contemporary consumer electronics, a significant challenge arises from the mismatch between the microscale of optics and the nanoscale of modern electronic devices, resulting in penalties related to power dissipation, area, noise, and latency (*81*). To address this, an efficient approach involves employing MIPDs to enhance photoelectric conversion efficiency using meta-atoms,

thereby improving light harvesting and enabling subwavelength active areas. In alignment with general units in electronics, such as transistors, memory, and logic components, metal nanoantennas can e.g. be combined with doped semiconductors to form Schottky photodiodes and play a dual electronic and optical function. Light from free space can excite plasmons in the metal nanoantenna (*82*), concentrating the light and enhancing the generation of hot electrons and nanoscale thermosplasmonic effects (*83*). For example, gold nanoantennas were used to concentrate near-infrared light into a subwavelength germanium photodetector, significantly enhancing its performance (*81*). The Schottky photodiode can also be simplified using a hybrid silicon-aluminum nanostructure to realize submicrometer pixel dimensions as shown in Fig. 6A (*84*). The design utilizes hybrid Mie-plasmon resonances to achieve color-selective light absorption, which is highly localized within the silicon nanocylinders. This localization minimizes the distance between color filters and the photodetector elements, reducing optical cross-talk that typically occurs when light from one filter is absorbed by neighboring photodetectors.

To obtain the spectral information rather than the simple integral of the incident broadband light into a single current value, spectroscopy is necessary, typically requiring wavelength selectivity and a detector. Metasurfaces facilitate the construction of ultracompact and lightweight spectrometers with solely detector arrays. For example, structurally-coloured, doped, vertical silicon nanowire arrays allow the engineering of responsivity spectra in a single chip, combining wavelength selectivity and photodetection functions as shown in Fig. 6B. This architecture enables spectral reconstruction of an unknown light source based on an algorithm that considers the measured photocurrents from the pixels and a library of their responsivity spectra (*85*). By manipulating the radiative coupling between horizontally-arrayed silicon nanowires, imperceptible photodetectors onto transparent substrates can be realized, opening a promising platform for augmented reality, wearables, and sensing applications (*86*). This strategy could overcome the disadvantages of traditional color sensors based on organic dye filters regarding durability, low efficiency, and fabrication complexity. Compact devices for video rate hyperspectral imaging with high-definition spatial and spectral resolution can be further made for portable applications like food safety, disease diagnosis, remote sensing, environmental monitoring, and artwork analysis (*87*).

In addition to spectral detection, polarization can be easily detected by breaking the four-fold rotational symmetry of meta-atoms using rectangular or elliptical shapes. The incident light with varying polarization states excites distinct resonances, resulting in different absorption and photocurrent values (*88*). Combining engineered chiral plasmonic metasurfaces with semiconductors enables the realization of an ultracompact circularly polarized light detector without additional optical elements (*89*). Full-Stokes detection is achieved by three-ports polarimeters comprising on-chip chiral plasmonic MIPDs. By manipulating the spatial distribution of chiral meta-atoms, polarization-resolved absorption information can be converted into corresponding polarization-resolved currents of three ports, facilitating reliable polarization reconstruction (*90*). Recently, it was shown how the incorporation of a metasurface diffraction grating into a machine vision imaging system can enable full-Stokes imaging polarimetry.(*91*) As

shown in Fig. 6C, an artificial bulk photovoltaic effect can be mimicked to realize cascaded polarization-sensitive photoresponse under uniform illumination with graphene-MIPDs for zero-bias uncooled mid-infrared applications. The vectorial photocurrent enables the detection of polarization angle with a single device regardless of the incident power, and its high responsivity holds great potential for exceeding the Shockley-Queisser limit in efficiency (*92*).

Inspired by natural design, electrically-isolated but optically-coupled Si nanowires can form a subwavelength photodetection pixel that can measure both the intensity and incident angle of light in a highly accurate fashion (Fig. 6D). This capability arises from the non-Hermitian optical coupling of the Mie resonances supported by the wires that causes measurable differences in the photocurrents from the wires that depend on the incident angle (*93*). With a sophisticated arrangement of the unit, direct wavefront detection becomes possible, offering advantages such as high spatial resolution, robustness, and high speed. This enables unprecedented capabilities such as video-frame recording of high-resolution surface topography (*94*).

Additionally, the property of OAM in light holds great promise for enhancing the bandwidth of optical communication networks. However, direct detection of different OAM modes poses a significant challenge, as most existing studies focus primarily on optical intensity-related effects, thereby losing crucial phase information. By combining tungsten ditelluride (WTe_2) with precisely engineered U-shaped electrode geometries (Fig. 6E), it becomes possible to directly characterize the topological charge of the incident OAM beam. The helical phase gradient drives the orbital photogalvanic effect, resulting in a photocurrent that directly reflects different OAM modes. This approach enables the detection of both scalar and vectorial OAM beams, allowing for a determination of the OAM order or the coordinates of any arbitrary OAM state on a higher-order Poincaré sphere. Through photocurrent measurement via a small matrix of electrodes, including arbitrary OAM mixtures, the nonlocal orbital photogalvanic effect holds significant potential for advancing the development of high-capacity optical chips and next-generation photoelectronic circuits (*95*).

Beyond the functionalities realized with individual units, arranging these single functional units into specific layouts and arrays can also enhance the efficiency and enable direct imaging of various properties of the light field as shown in Fig. 6F. In addition, through sophisticated integration and co-design with methods such as machine learning or inverse design, multifunctional photodetectors can be achieved in near-field or far-field configurations for applications in spectropolarimeters, angle-resolved spectrometers (*96*), superconducting single-photon spectrometers (*97*), etc. Optical computing with metasurfaces is currently an active area of research, typically captured by imaging the calculated results from the metasurface with a photodetector (*98*). Further development could enable direct optoelectronic conversion, achieving optoelectronic computing fusion for applications such as edge extraction and super-resolution reconstruction. This would allow single-shot real-time decision-making with a meta-imager (*99*), reducing heavy computational demands and energy consumption in machine vision technology, with potential applications in medical devices and autonomous driving systems. (*98*)

It is worth noting that a recent breakthrough of low-dimensional materials (LDMs) in optics and electronics offers new possibilities when combined with MIPDs (*100*). Benefitting from the enhanced absorption with metasurfaces, emerging materials such as boron nitride, graphene, and transition metal dichalcogenides with band gaps covering a wide spectral range from ultraviolet to terahertz may broaden the applications for weak light detection and flexible and wearable optoelectronics (*101*). These materials lend themselves nicely to metasurface integration, either through directly creating nanostructures in them or by ensuring mode overlap with metasurfaces patterned in other materials. The incorporation of LDMs paves the way for photodetectors driven by electronics towards the "more than Moore's" or "beyond Moore's" era.

Future development of MIPDs includes the exploration of new design methods with different physical principles, selecting suitable materials, including quantum dots and perovskite nanocrystals, for specific band applications with structurally-enhanced sensitivity, high signal-to-noise ratios, fast response speeds, stability in various environments, etc. Enhancements in signal extraction, calibration, denoising, and analysis are also essential. The functions powered by metasurfaces can be further improved, such as high-efficiency imaging with color routers, direct photoelectric 3D imaging, and complex amplitude imaging. Beyond the classical domain, MIPDs can potentially be used for photon number count and quantum state detection in the quantum domain (*25*). Considering practical industrial applications, miniaturized MIPDs have significant potential for portable applications such as consumer electronics, health care, and manufacturing, demanding lightweight, high spectral resolution, sufficient spatial resolution, and fast refresh rates. The fabrication technique should be CMOS compatible, enabling seemless ultracompact planar integration and mass production at low cost. With the key advantages of metasurfaces for ultimate miniaturization, empowering novel functionalities tprocess various properties of light, and the opportunity to tune their properties on demand, it is expected that MIPDs will enable smart vision, foreseeing a revolution in the photoelectric detection and imaging of light with multidimensional information (*102*).

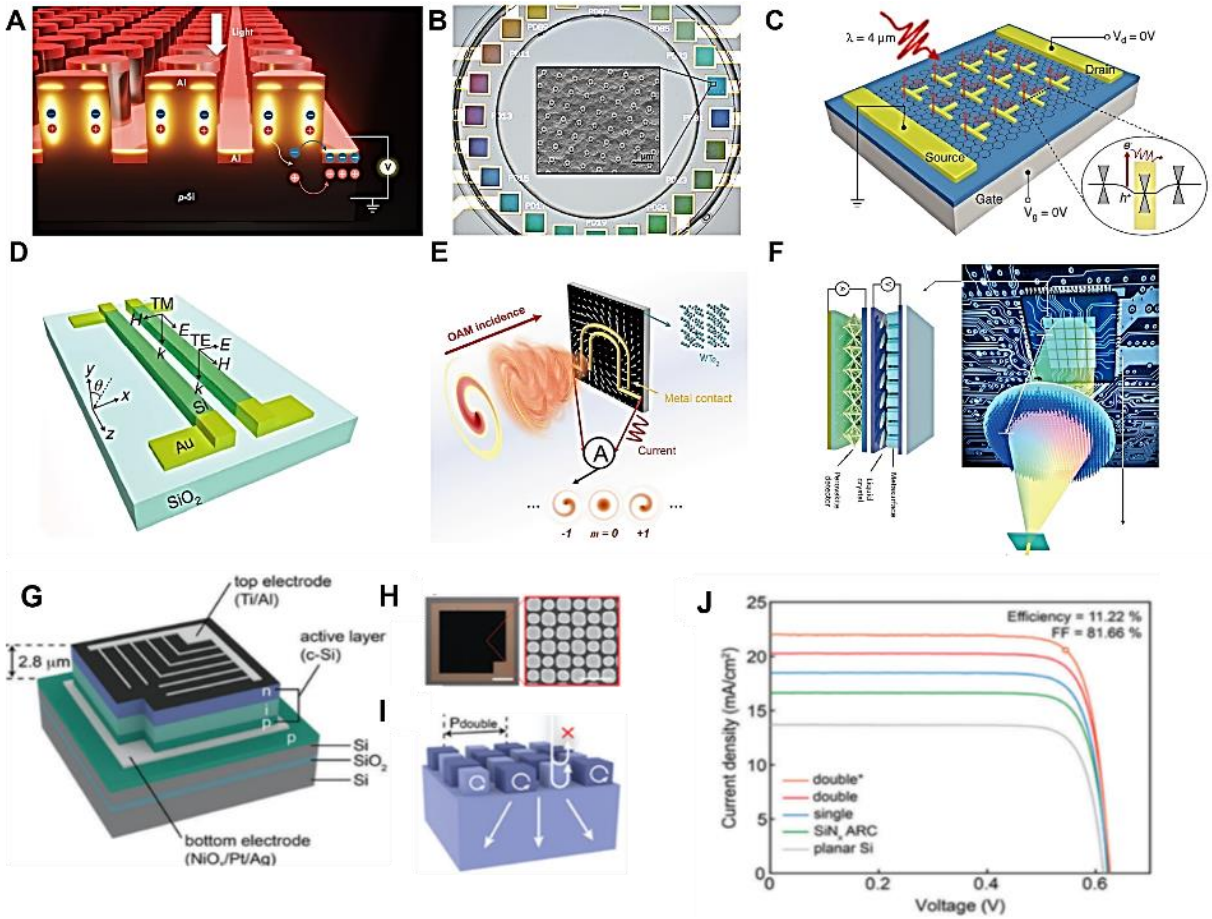

Fig. 6. Metasurface-based photodetectors and solar cells. (**A**) Schematic of the Al-Si hybrid color-selective photodetector (*84*). (**B**) Photograph of a device mounted in a chip with 24 different structure-colored Si nanowire photodetectors with various diameters for spectral measurement. Inset shows SEM image of one patch of nanowires embedded in the photoresist layer (*85*). (**C**) Illustration of the graphene-MIPDs consisting of non-centrosymmetric sub-wavelength metallic nanoantennas on top of graphene flakes. Global directional photocurrent can be generated at zero external bias to mimic the shift current in the bulk photovoltaic effect for polarization detection (*92*). (**D**) Unit of angle-sensing photodetector with a pair of Si nanowires connected with Au contacts (*93*). (**E**) Illustration for OAM detection with photocurrent measurement by U-shaped electrodes on WTe_2 (*95*). (**F**) Compact angle-resolved metasurface spectrometer consisting of liquid-crystal-infiltrated metasurface integrated with perovskite photodetectors (*96*). (**G**) Schematic of an ultrathin solar cell integrated with nanostructured light-trapping antireflection coating (LARC) shown as the dark region in the schematic . (**H**) White-light optical micrograph image (left) and scanning electron microscopy (SEM) image (right) of the top surface of the c-Si solar cell in (G) that appears dark due to the LARC structures. (**I**) A schematic of a LARC structure comprised of nanoscale Mie resonators with a bi-modal size distribution (**J**) Current-voltage characteristics of 2.8-μm-thick Si solar cells with different types of photon management schemes: a LARC with a bi-modal size distribution of Mie-resonators (red), a single-sized Mie-resonant ARC (blue), a conventional SiNx ARC (green), and a planar cell without an ARC (grey). The orange curve shows the highest efficiency cell with a bi-modal LARC on a different wafer. Cells with low surface recombination velocities and high efficiencies (η = 11.22%) can be realized, showing the promise of metasurface-based light trapping strategies. (G – J) from (*103*).

Thin-film Solar cells

Solar cells capitalize on the special electronic and optical properties of semiconductors to convert sunlight into clean electrical power. These materials display high refractive indices and a polished semiconductor surface therefore strongly reflecting light. For this reason, transparent layers of dielectrics or conductive oxides/polymers are applied as antireflection coatings to let the light into the cell. Most cells also employ light-trapping structures to redirect incident photons into the plane of the cell to boost absorption. On thicker cells, light trapping is achieved with macroscopic, micron-scale structures and those can deliver power conversion efficiencies as high as 25% for crystalline silicon (c-Si) cells (*104*), the most widely used photovoltaic technology today. However, significant research and development is currently aimed at exploring ways to reduce the materials usage, weight, and production cost of solar modules. There is also a drive towards increased flexibility. Thin-film cells from a variety of semiconductor materials may provide a viable pathway towards this goal. If proper light trapping strategies can be developed, they could enable the realization of ultrahigh-efficiency thin cells at low cost and provide the ultimate solution for utility-scale solar. They can also open new application spaces in robotics, aerospace, transportation, internet of things sensors, and wearable devices (*105*).

The conventional macroscopic surface textures commonly applied on thick crystalline cells are not suited for thin devices particularly when the cell thickness is comparable or smaller than macroscopic texture size. Here, the implementation of nanostructured light trapping layers is proving to be more effective. Both plasmonic (*106–110*) and Mie-resonant (*103, 111–115*) light-trapping layers have been developed. Plasmonic anti-reflection and light-trapping layers always suffer from some unwanted optical absorption losses in the metal. Despite such losses, structured plasmonic back reflectors have been able to deliver power conversion efficiencies comparable to world records in certain materials systems (e.g. dye-sensitized solar cells (*116*)). In this case, the light can have one pass through the solar cell before interacting with the lossy metal. In many solar cells, metallic back contacts are used for the extraction of photocurrent, and adding nanopatterns for light trapping can be beneficial.

Mie-resonant structures can be patterned directly on semiconductor layers, and therefore offer similar light scattering and light trapping functions but do not suffer from the parasitic losses. Mie-resonant antireflection coatings (ARCs) have already been realized at wafer scale (*111*) and the palette of large-area nanopatterning techniques for metasurfaces is rapidly expanding and includes various soft lithography, immersion lithography, nanoimprint lithography, and advanced semiconductor manufacturing technology approaches (*117–122*). In such ARCs, the scattering from the nanostructures can effectively cancel the unwanted reflection from a high-index semiconductor substrate through destructive interference. It was recently shown that the introduction of a bi-modal size distribution can be used to create light-trapping ARCs (LARCs) where the resonances in the differently sized elements can work together to achieve both effective antireflection and light trapping functions across the broad solar spectrum (*103, 123*). In this application co-design of the electronic and optical properties is critical. The Mie resonators offer light trapping if properly

sized. At the same time a thin, high-quality surface passivation layer is needed for such nanopatterned surfaces through thermal oxidation to achieve high power conversion efficiencies. Figures 6 G-J show how very thin cells supplied with Mie-resonant LARCs can produce notable power conversion efficiency for few-micron thick cells (e.g. 11.2% for a sub-3-μm-thick c-Si solar cell) (*103*).

Perspective and future outlooks

The direct integration of metasurfaces in optoelectronic devices is poised to deliver transformative advances. As the field evolves, we can anticipate a surge in the development of ultra-compact, highly-efficient, and multi-functional devices that leverage the unique light-manipulating capabilities of metasurfaces (*59, 124*). However, realizing this potential requires a careful co-design approach where both the photonic and electronic functionalities are optimized in tandem. Metadevices, which simultaneously demand high photonic performance and efficient electronic operation, present unique challenges that necessitate a balanced consideration of both domains. In particular, metasurfaces integrated into optoelectronic devices must strike a delicate balance between controlling light at the nanoscale and maintaining efficient electronic functionality, such as charge injection, field application, and thermal management. Co-design efforts are essential to ensure that while metasurfaces enhance light manipulation (e.g., beam steering, polarization control, or wavelength selectivity), the electronic aspects of the device are not compromised. The photonic and electronic systems must be designed in harmony, from the layout of the nanoresonators to the configuration of electrodes, to avoid issues like current crowding, excessive resistance, or unwanted thermal effects.

Moreover, the integration of metasurfaces into optoelectronic devices must consider the choice of materials and device architecture. Metadevices can incorporate a variety of materials, each with unique optical and electronic properties. For instance, while high-index dielectric materials like silicon can achieve strong light-matter interaction through Mie resonances, careful attention must be paid to the material's compatibility with the electronic layers. The overall device configuration, such as the placement of metasurfaces relative to the active layers and electrodes, plays a critical role in optimizing both light manipulation and electronic performance.

Finally, to bring these metadevices to commercial fruition, large-scale nanopatterning techniques that are compatible with industrial standards are indispensable. Scalability remains a significant challenge for metasurface technologies. Developing manufacturing processes that can reliably produce large-area metasurfaces with subwavelength precision is critical (*125–127*). Techniques like nanoimprint lithography or photolithography supported by advanced semiconductor manufacturing technologies will need to be adapted and refined for high-throughput production, ensuring that metasurface-integrated devices can meet the demands of industrial applications. Looking ahead, collaborative efforts across disciplines, bridging photonics, electronics, materials science, and manufacturing, will be key to overcoming these challenges. The co-design approach, in particular, will be instrumental in realizing the full potential of metasurface-based optoelectronic

devices. Additionally, strong partnerships between academia and industry, where scientists and engineers work together, will be crucial for translating research innovations into commercially viable metadevices. These efforts promise to unlock new possibilities in fields ranging from advanced sensors and imaging systems to next-generation displays, optical computing, and quantum technologies.

References

1. G. Wetzstein, A. Ozcan, S. Gigan, S. Fan, D. Englund, M. Soljačić, C. Denz, D. A. B. Miller, D. Psaltis, Inference in artificial intelligence with deep optics and photonics. *Nature* **588**, 39–47 (2020).
2. E. Strubell, A. Ganesh, A. McCallum, Energy and policy considerations for modern deep learning research. *AAAI 2020 - 34th AAAI Conference on Artificial Intelligence*, 13693–13696 (2020).
3. A. Andrae, Comparison of Several Simplistic High-Level Approaches for Estimating the Global Energy and Electricity Use of ICT Networks and Data Centers. *International Journal of Green Technology* **5**, 50–63 (2019).
4. J. A. Schuller, E. S. Barnard, W. Cai, Y. C. Jun, J. S. White, M. L. Brongersma, Plasmonics for extreme light concentration and manipulation. *Nat Mater* **9**, 193–204 (2010).
5. A. I. Kuznetsov, A. E. Miroshnichenko, M. L. Brongersma, Y. S. Kivshar, B. Luk'yanchuk, Optically resonant dielectric nanostructures. *Science* **354** (2016).
6. W. Joo, J. Kyoung, M. Esfandyarpour, S. Lee, H. Koo, S. Song, Y. Kwon, S. H. Song, J. C. Bae, A. Jo, M. Kwon, S. H. Han, S. Kim, S. Hwang, M. L. Brongersma, Metasurface-driven OLED displays beyond 10,000 pixels per inch. *Science* **370**, 459–463 (2020).
7. M. Esfandyarpour, E. C. Garnett, Y. Cui, M. D. McGehee, M. L. Brongersma, Metamaterial mirrors in optoelectronic devices. *Nat Nanotechnol* **9**, 542–547 (2014).
8. T. Nikolajsen, K. Leosson, S. I. Bozhevolnyi, Surface plasmon polariton based modulators and switches operating at telecom wavelengths. *Appl Phys Lett* **85**, 5833–5835 (2004).
9. Q. Li, J. H. Song, F. Xu, J. van de Groep, J. Hong, A. Daus, Y. J. Lee, A. C. Johnson, E. Pop, F. Liu, M. L. Brongersma, A Purcell-enabled monolayer semiconductor free-space optical modulator. *Nat Photonics* **17** (2023).
10. J. C. Prangsma, J. Kern, A. G. Knapp, S. Grossmann, M. Emmerling, M. Kamp, B. Hecht, Electrically connected resonant optical antennas. *Nano Lett* **12**, 3915–3919 (2012).
11. K. C. Y. Huang, M.-K. Seo, Y. Huo, T. Sarmiento, J. S. Harris, M. L. Brongersma, Antenna electrodes for controlling electroluminescence. *Nat Commun* **3**, 1005 (2012).
12. M. Esfandyarpour, A. G. Curto, P. G. Kik, N. Engheta, M. L. Brongersma, Optical emission near a high-impedance mirror. *Nat Commun* **9**, 3324 (2018).
13. A. M. Shaltout, J. Kim, A. Boltasseva, V. M. Shalaev, A. V. Kildishev, Ultrathin and multicolour optical cavities with embedded metasurfaces. *Nat Commun* **9**, 1–7 (2018).
14. D. Sievenpiper, L. Z. L. Zhang, R. F. J. Broas, N. G. Alexopolous, E. Yablonovitch, High-impedance electromagnetic surfaces with a forbidden frequency band. *IEEE Trans Microw Theory Tech* **47** (1999).
15. A. Schwanecke, V. Fedotov, V. Khardikov, S. Prosvirnin, Y. Chen, N. I. Zheludev, Optical magnetic mirrors. *Journal of Optics A: Pure and Applied Optics* **9**, L1–L2 (2007).
16. W. Cai, J. S. White, M. L. Brongersma, Compact, High-Speed and Power-Efficient Electrooptic Plasmonic Modulators. *Nano Lett* (2009).
17. S. J. Kim, P. Fan, J.-H. Kang, M. L. Brongersma, Creating semiconductor metafilms with designer absorption spectra. *Nat Commun* **6**, 7591 (2015).
18. L. Cao, J. S. White, J.-S. Park, J. a Schuller, B. M. Clemens, M. L. Brongersma, Engineering light absorption in semiconductor nanowire devices. *Nat Mater* **8**, 643–647 (2009).
19. L. Cao, P. Fan, E. S. Barnard, A. M. Brown, M. L. Brongersma, Tuning the color of silicon nanostructures. *Nano Lett* **10**, 2649–2654 (2010).
20. Q. Li, J. van de Groep, A. K. White, J. H. Song, S. A. Longwell, P. M. Fordyce, S. R. Quake, P. G. Kik, M. L. Brongersma, Metasurface optofluidics for dynamic control of light fields. *Nat Nanotechnol* **17**, 1097–1103 (2022).

21. E. Khaidarov, Z. Liu, R. Paniagua-Domínguez, S. T. Ha, V. Valuckas, X. Liang, Y. Akimov, P. Bai, C. E. Png, H. V. Demir, A. I. Kuznetsov, Control of LED Emission with Functional Dielectric Metasurfaces. *Laser Photon Rev* **14**, 1900235 (2020).
22. P. Mao, C. Liu, X. Li, M. Liu, Q. Chen, M. Han, S. A. Maier, E. H. Sargent, S. Zhang, Single-step-fabricated disordered metasurfaces for enhanced light extraction from LEDs. *Light Sci Appl* **10**, 180 (2021).
23. P. P. Iyer, R. A. DeCrescent, Y. Mohtashami, G. Lheureux, N. A. Butakov, A. Alhassan, C. Weisbuch, S. Nakamura, S. P. DenBaars, J. A. Schuller, Unidirectional luminescence from InGaN/GaN quantum-well metasurfaces. *Nat Photonics* **14**, 543–548 (2020).
24. W. T. Chen, A. Y. Zhu, F. Capasso, Flat optics with dispersion-engineered metasurfaces. *Nat Rev Mater* **5**, 604–620 (2020).
25. A. S. Solntsev, G. S. Agarwal, Y. S. Kivshar, Metasurfaces for quantum photonics. *Nat Photonics* **15**, 327–336 (2021).
26. A. Vaskin, R. Kolkowski, A. F. Koenderink, I. Staude, Light-emitting metasurfaces. *Nanophotonics* **8**, 1151–1198 (2019).
27. J. Yun, H. Hirayama, Investigation of Light-Extraction Efficiency of Flip-Chip AlGaN-Based Deep-Ultraviolet Light-Emitting Diodes Adopting AlGaN Metasurface. *IEEE Photonics J* **13**, 2700313 (2021).
28. Z. Hu, C. Liu, G. Li, Disordered optical metasurfaces: from light manipulation to energy harvesting. *Adv Phys X* **8** (2023).
29. P. Lalanne, M. Chen, C. Rockstuhl, A. Sprafke, A. Dmitriev, K. Vynck, Disordered optical metasurfaces: basics, design and applications. *arXiv:2408.09425* (2024).
30. P. P. Iyer, N. Karl, S. Addamane, S. D. Gennaro, M. B. Sinclair, I. Brener, Sub-picosecond steering of ultrafast incoherent emission from semiconductor metasurfaces. *Nat Photonics* **17**, 588–593 (2023).
31. S. T. Ha, Y. H. Fu, N. K. Emani, Z. Pan, R. M. Bakker, R. Paniagua-Domínguez, A. I. Kuznetsov, Directional lasing in resonant semiconductor nanoantenna arrays. *Nat Nanotechnol* **13**, 1042–1047 (2018).
32. X. Zhang, Y. Liu, J. Han, Y. Kivshar, Q. Song, Chiral emission from resonant metasurfaces. *Science* **377**, 1215–1218 (2022).
33. H.-Y. Luan, Y.-H. Ouyang, Z.-W. Zhao, W.-Z. Mao, R.-M. Ma, Reconfigurable moiré nanolaser arrays with phase synchronization. *Nature* **624**, 282–288 (2023).
34. K. Hirose, Y. Liang, Y. Kurosaka, A. Watanabe, T. Sugiyama, S. Noda, Watt-class high-power, high-beam-quality photonic-crystal lasers. *Nat Photonics* **8**, 406–411 (2014).
35. A. S. D. Sandanayaka, T. Matsushima, F. Bencheikh, S. Terakawa, W. J. Potscavage, C. Qin, T. Fujihara, K. Goushi, J.-C. Ribierre, C. Adachi, Indication of current-injection lasing from an organic semiconductor. *Applied Physics Express* **12**, 061010 (2019).
36. J. Roh, Y.-S. Park, J. Lim, V. I. Klimov, Optically pumped colloidal-quantum-dot lasing in LED-like devices with an integrated optical cavity. *Nat Commun* **11**, 271 (2020).
37. W. Zhou, M. Dridi, J. Y. Suh, C. H. Kim, D. T. Co, M. R. Wasielewski, G. C. Schatz, T. W. Odom, Lasing action in strongly coupled plasmonic nanocavity arrays. *Nat Nanotechnol* **8**, 506–511 (2013).
38. Y. Liang, D. P. Tsai, Y. Kivshar, From Local to Nonlocal High-Q Plasmonic Metasurfaces. *Phys Rev Lett* **133**, 053801 (2024).
39. D. A. Bykov, E. A. Bezus, L. L. Doskolovich, Coupled-wave formalism for bound states in the continuum in guided-mode resonant gratings. *Phys Rev A (Coll Park)* **99**, 063805 (2019).
40. S. T. Ha, R. Paniagua-Domínguez, A. I. Kuznetsov, Room-Temperature Multi-Beam, Multi-Wavelength Bound States in the Continuum Laser. *Adv Opt Mater* **10**, 2200753 (2022).
41. J. Jin, X. Yin, L. Ni, M. Soljačić, B. Zhen, C. Peng, Topologically enabled ultrahigh-Q guided resonances robust to out-of-plane scattering. *Nature* **574**, 501–504 (2019).
42. M.-S. Hwang, H.-C. Lee, K.-H. Kim, K.-Y. Jeong, S.-H. Kwon, K. Koshelev, Y. Kivshar, H.-G. Park, Ultralow-threshold laser using super-bound states in the continuum. *Nat Commun* **12**, 4135 (2021).
43. Z. Chen, X. Yin, J. Jin, Z. Zheng, Z. Zhang, F. Wang, L. He, B. Zhen, C. Peng, Observation of miniaturized bound states in the continuum with ultra-high quality factors. *Sci Bull (Beijing)* **67**, 359–366 (2022).
44. C. Huang, C. Zhang, S. Xiao, Y. Wang, Y. Fan, Y. Liu, N. Zhang, G. Qu, H. Ji, J. Han, L. Ge, Y. Kivshar, Q. Song, Ultrafast control of vortex microlasers. *Science* **367**, 1018–1021 (2020).
45. Y. Chen, H. Deng, X. Sha, W. Chen, R. Wang, Y.-H. Chen, D. Wu, J. Chu, Y. S. Kivshar, S. Xiao, C.-W. Qiu, Observation of intrinsic chiral bound states in the continuum. *Nature* **613**, 474–478 (2023).
46. Y.-H. Ouyang, H.-Y. Luan, Z.-W. Zhao, W.-Z. Mao, R.-M. Ma, Singular dielectric nanolaser with atomic-scale field localization. *Nature* **632**, 287–293 (2024).
47. R. Contractor, W. Noh, W. Redjem, W. Qarony, E. Martin, S. Dhuey, A. Schwartzberg, B. Kanté, Scalable single-mode surface-emitting laser via open-Dirac singularities. *Nature* **608**, 692–698 (2022).

48. M. P. Hokmabadi, N. S. Nye, R. El-Ganainy, D. N. Christodoulides, M. Khajavikhan, Supersymmetric laser arrays. *Science* **363**, 623–626 (2019).
49. M. A. Bandres, S. Wittek, G. Harari, M. Parto, J. Ren, M. Segev, D. N. Christodoulides, M. Khajavikhan, Topological insulator laser: Experiments. *Science* **359** (2018).
50. Y. Zeng, U. Chattopadhyay, B. Zhu, B. Qiang, J. Li, Y. Jin, L. Li, A. G. Davies, E. H. Linfield, B. Zhang, Y. Chong, Q. J. Wang, Electrically pumped topological laser with valley edge modes. *Nature* **578**, 246–250 (2020).
51. B. Bahari, A. Ndao, F. Vallini, A. El Amili, Y. Fainman, B. Kanté, Nonreciprocal lasing in topological cavities of arbitrary geometries. *Science* **358**, 636–640 (2017).
52. H. Hodaei, M.-A. Miri, M. Heinrich, D. N. Christodoulides, M. Khajavikhan, Parity-time–symmetric microring lasers. *Science* **346**, 975–978 (2014).
53. M. Yoshida, S. Katsuno, T. Inoue, J. Gelleta, K. Izumi, M. De Zoysa, K. Ishizaki, S. Noda, High-brightness scalable continuous-wave single-mode photonic-crystal laser. *Nature* **618**, 727–732 (2023).
54. K. Yoshida, J. Gong, A. L. Kanibolotsky, P. J. Skabara, G. A. Turnbull, I. D. W. Samuel, Electrically driven organic laser using integrated OLED pumping. *Nature* **621**, 746–752 (2023).
55. N. Ahn, C. Livache, V. Pinchetti, H. Jung, H. Jin, D. Hahm, Y.-S. Park, V. I. Klimov, Electrically driven amplified spontaneous emission from colloidal quantum dots. *Nature* **617**, 79–85 (2023).
56. Y.-S. Park, J. Roh, B. T. Diroll, R. D. Schaller, V. I. Klimov, Colloidal quantum dot lasers. *Nat Rev Mater* **6**, 382–401 (2021).
57. R. Paniagua-Dominguez, S. T. Ha, A. I. Kuznetsov, Active and Tunable Nanophotonics With Dielectric Nanoantennas. *Proceedings of the IEEE* **108**, 749–771 (2020).
58. A. M. Shaltout, V. M. Shalaev, M. L. Brongersma, Spatiotemporal light control with active metasurfaces. *Science* **364**, eaat3100 (2019).
59. A. I. Kuznetsov, M. L. Brongersma, J. Yao, M. K. Chen, U. Levy, D. P. Tsai, N. I. Zheludev, A. Faraon, A. Arbabi, N. Yu, D. Chanda, K. B. Crozier, A. V. Kildishev, H. Wang, J. K. W. Yang, J. G. Valentine, P. Genevet, J. A. Fan, O. D. Miller, A. Majumdar, J. E. Fröch, D. Brady, F. Heide, A. Veeraraghavan, N. Engheta, A. Alù, A. Polman, H. A. Atwater, P. Thureja, R. Paniagua-Dominguez, S. T. Ha, A. I. Barreda, J. A. Schuller, I. Staude, G. Grinblat, Y. Kivshar, S. Peana, S. F. Yelin, A. Senichev, V. M. Shalaev, S. Saha, A. Boltasseva, J. Rho, D. K. Oh, J. Kim, J. Park, R. Devlin, R. A. Pala, Roadmap for Optical Metasurfaces. *ACS Photonics*, doi: 10.1021/acsphotonics.3c00457 (2024).
60. P. Thureja, R. Sokhoyan, C. U. Hail, J. Sisler, M. Foley, M. Y. Grajower, H. A. Atwater, Toward a universal metasurface for optical imaging, communication, and computation. *Nanophotonics* **11**, 3745–3768 (2022).
61. P. Moitra, X. Xu, R. Maruthiyodan Veetil, X. Liang, T. W. W. Mass, A. I. Kuznetsov, R. Paniagua-Domínguez, Electrically Tunable Reflective Metasurfaces with Continuous and Full-Phase Modulation for High-Efficiency Wavefront Control at Visible Frequencies. *ACS Nano* **17**, 16952–16959 (2023).
62. A. Komar, Z. Fang, J. Bohn, J. Sautter, M. Decker, A. Miroshnichenko, T. Pertsch, I. Brener, Y. S. Kivshar, I. Staude, D. N. Neshev, Electrically tunable all-dielectric optical metasurfaces based on liquid crystals. *Appl Phys Lett* **110**, 071109 (2017).
63. S.-Q. Li, X. Xu, R. Maruthiyodan Veetil, V. Valuckas, R. Paniagua-Domínguez, A. I. Kuznetsov, Phase-only transmissive spatial light modulator based on tunable dielectric metasurface. *Science* **364**, 1087–1090 (2019).
64. Y. Zhang, C. Fowler, J. Liang, B. Azhar, M. Y. Shalaginov, S. Deckoff-Jones, S. An, J. B. Chou, C. M. Roberts, V. Liberman, M. Kang, C. Ríos, K. A. Richardson, C. Rivero-Baleine, T. Gu, H. Zhang, J. Hu, Electrically reconfigurable non-volatile metasurface using low-loss optical phase-change material. *Nat Nanotechnol* **16**, 661–666 (2021).
65. S. Abdollahramezani, O. Hemmatyar, M. Taghinejad, H. Taghinejad, A. Krasnok, A. A. Eftekhar, C. Teichrib, S. Deshmukh, M. A. El-Sayed, E. Pop, M. Wuttig, A. Alù, W. Cai, A. Adibi, Electrically driven reprogrammable phase-change metasurface reaching 80% efficiency. *Nat Commun* **13**, 1696 (2022).
66. Y. Wang, P. Landreman, D. Schoen, K. Okabe, A. Marshall, U. Celano, H.-S. P. Wong, J. Park, M. L. Brongersma, Electrical tuning of phase-change antennas and metasurfaces. *Nat Nanotechnol* **16**, 667–672 (2021).
67. C. C. Popescu, K. Aryana, P. Garud, K. P. Dao, S. Vitale, V. Liberman, H. Bae, T. Lee, M. Kang, K. A. Richardson, M. Julian, C. A. R. Ocampo, Y. Zhang, T. Gu, J. Hu, H. J. Kim, Electrically Reconfigurable Phase-Change Transmissive Metasurface. *Advanced Materials*, doi: 10.1002/adma.202400627 (2024).
68. Z. Fang, R. Chen, J. E. Fröch, Q. A. A. Tanguy, A. I. Khan, X. Wu, V. Tara, A. Manna, D. Sharp, C. Munley, F. Miller, Y. Zhao, S. Geiger, K. F. Böhringer, M. S. Reynolds, E. Pop, A. Majumdar, Nonvolatile

Phase-Only Transmissive Spatial Light Modulator with Electrical Addressability of Individual Pixels. *ACS Nano* **18**, 11245–11256 (2024).
69. S. Il Kim, J. Park, B. G. Jeong, D. Lee, K.-Y. Yang, Y.-Y. Park, K. Ha, H. Choo, Two-dimensional beam steering with tunable metasurface in infrared regime. *Nanophotonics* **11**, 2719–2726 (2022).
70. J. Park, B. G. Jeong, S. Il Kim, D. Lee, J. Kim, C. Shin, C. B. Lee, T. Otsuka, J. Kyoung, S. Kim, K.-Y. Yang, Y.-Y. Park, J. Lee, I. Hwang, J. Jang, S. H. Song, M. L. Brongersma, K. Ha, S.-W. Hwang, H. Choo, B. L. Choi, All-solid-state spatial light modulator with independent phase and amplitude control for three-dimensional LiDAR applications. *Nat Nanotechnol* **16**, 69–76 (2021).
71. G. K. Shirmanesh, R. Sokhoyan, P. C. Wu, H. A. Atwater, Electro-optically Tunable Multifunctional Metasurfaces. *ACS Nano* **14**, 6912–6920 (2020).
72. Y.-W. Huang, H. W. H. Lee, R. Sokhoyan, R. A. Pala, K. Thyagarajan, S. Han, D. P. Tsai, H. A. Atwater, Gate-Tunable Conducting Oxide Metasurfaces. *Nano Lett* **16**, 5319–5325 (2016).
73. S. Wang, P. C. Wu, V.-C. Su, Y.-C. Lai, M.-K. Chen, H. Y. Kuo, B. H. Chen, Y. H. Chen, T.-T. Huang, J.-H. Wang, R.-M. Lin, C.-H. Kuan, T. Li, Z. Wang, S. Zhu, D. P. Tsai, A broadband achromatic metalens in the visible. *Nat Nanotechnol* **13**, 227–232 (2018).
74. M. L. Tseng, M. Semmlinger, M. Zhang, C. Arndt, T.-T. Huang, J. Yang, H. Y. Kuo, V.-C. Su, M. K. Chen, C. H. Chu, B. Cerjan, D. P. Tsai, P. Nordlander, N. J. Halas, Vacuum ultraviolet nonlinear metalens. *Sci Adv* **8** (2022).
75. T. Gu, H. J. Kim, C. Rivero-Baleine, J. Hu, Reconfigurable metasurfaces towards commercial success. *Nat Photonics* **17**, 48–58 (2023).
76. A. I. Kuznetsov, "Flat optics and nanoantenna spatial light modulators for imaging, LiDAR, and 3D holographic display applications" in *High Contrast Metastructures XIII*, C. J. Chang-Hasnain, W. Zhou, A. Alù, Eds. (SPIE, 2024), p. PC128970E.
77. HOLOEYE Photonics AG, GAEA-2 Spatial Light Modulators, *https://holoeye.com/products/spatial-light-modulators/gaea-2-phase-only/* .
78. J. Karst, M. Floess, M. Ubl, C. Dingler, C. Malacrida, T. Steinle, S. Ludwigs, M. Hentschel, H. Giessen, Electrically switchable metallic polymer nanoantennas. *Science* **374**, 612–616 (2021).
79. Y. Lee, J. Karst, M. Ubl, M. Hentschel, H. Giessen, Dynamic beam control based on electrically switchable nanogratings from conducting polymers. *Nanophotonics* **12**, 2865–2871 (2023).
80. R. Kaissner, J. Li, W. Lu, X. Li, F. Neubrech, J. Wang, N. Liu, Electrochemically controlled metasurfaces with high-contrast switching at visible frequencies. *Sci Adv* **7**, eabd9450 (2021).
81. L. Tang, S. E. Kocabas, S. Latif, A. K. Okyay, D.-S. Ly-Gagnon, K. C. Saraswat, D. A. B. Miller, Nanometre-scale germanium photodetector enhanced by a near-infrared dipole antenna. *Nat Photonics* **2**, 226–229 (2008).
82. M. W. Knight, H. Sobhani, P. Nordlander, N. J. Halas, Photodetection with Active Optical Antennas. *Science* **332**, 702–704 (2011).
83. K.-T. Lin, H. Lin, B. Jia, Plasmonic nanostructures in photodetection, energy conversion and beyond. *Nanophotonics* **9**, 3135–3163 (2020).
84. J. Ho, Z. Dong, H. S. Leong, J. Zhang, F. Tjiptoharsono, S. Daqiqeh Rezaei, K. C. H. Goh, M. Wu, S. Li, J. Chee, C. P. Y. Wong, A. I. Kuznetsov, J. K. W. Yang, Miniaturizing color-sensitive photodetectors via hybrid nanoantennas toward submicrometer dimensions. *Sci Adv* **8**, eadd3868 (2022).
85. J. Meng, J. J. Cadusch, K. B. Crozier, Detector-Only Spectrometer Based on Structurally Colored Silicon Nanowires and a Reconstruction Algorithm. *Nano Lett* **20**, 320–328 (2020).
86. Q. Li, J. van de Groep, Y. Wang, P. G. Kik, M. L. Brongersma, Transparent multispectral photodetectors mimicking the human visual system. *Nat Commun* **10**, 4982 (2019).
87. M. Yako, Y. Yamaoka, T. Kiyohara, C. Hosokawa, A. Noda, K. Tack, N. Spooren, T. Hirasawa, A. Ishikawa, Video-rate hyperspectral camera based on a CMOS-compatible random array of Fabry–Pérot filters. *Nat Photonics* **17**, 218–223 (2023).
88. J. Hong, J. van de Groep, N. Lee, S. J. Kim, P. Lalanne, P. G. Kik, M. L. Brongersma, Nonlocal metasurface for circularly polarized light detection. *Optica* **10**, 134 (2023).
89. W. Li, Z. J. Coppens, L. V. Besteiro, W. Wang, A. O. Govorov, J. Valentine, Circularly polarized light detection with hot electrons in chiral plasmonic metamaterials. *Nat Commun* **6**, 8379 (2015).
90. M. Dai, C. Wang, B. Qiang, F. Wang, M. Ye, S. Han, Y. Luo, Q. J. Wang, On-chip mid-infrared photothermoelectric detectors for full-Stokes detection. *Nat Commun* **13**, 4560 (2022).
91. N. A. Rubin, P. Chevalier, M. Juhl, M. Tamagnone, R. Chipman, F. Capasso, Imaging polarimetry through metasurface polarization gratings. *Opt Express* **30**, 9389 (2022).

92. J. Wei, Y. Li, L. Wang, W. Liao, B. Dong, C. Xu, C. Zhu, K.-W. Ang, C.-W. Qiu, C. Lee, Zero-bias mid-infrared graphene photodetectors with bulk photoresponse and calibration-free polarization detection. *Nat Commun* **11**, 6404 (2020).
93. S. Yi, M. Zhou, Z. Yu, P. Fan, N. Behdad, D. Lin, K. X. Wang, S. Fan, M. Brongersma, Subwavelength angle-sensing photodetectors inspired by directional hearing in small animals. *Nat Nanotechnol* **13**, 1143–1147 (2018).
94. S. Yi, J. Xiang, M. Zhou, Z. Wu, L. Yang, Z. Yu, Angle-based wavefront sensing enabled by the near fields of flat optics. *Nat Commun* **12**, 6002 (2021).
95. Z. Ji, W. Liu, S. Krylyuk, X. Fan, Z. Zhang, A. Pan, L. Feng, A. Davydov, R. Agarwal, Photocurrent detection of the orbital angular momentum of light. *Science* **368**, 763–767 (2020).
96. G. Cai, Y. Li, Y. Zhang, X. Jiang, Y. Chen, G. Qu, X. Zhang, S. Xiao, J. Han, S. Yu, Y. Kivshar, Q. Song, Compact angle-resolved metasurface spectrometer. *Nat Mater* **23**, 71–78 (2024).
97. R. Cheng, C.-L. Zou, X. Guo, S. Wang, X. Han, H. X. Tang, Broadband on-chip single-photon spectrometer. *Nat Commun* **10**, 4104 (2019).
98. S. Colburn, A. Zhan, A. Majumdar, Metasurface optics for full-color computational imaging. *Sci Adv* **4** (2018).
99. H. Zheng, Q. Liu, I. I. Kravchenko, X. Zhang, Y. Huo, J. G. Valentine, Multichannel meta-imagers for accelerating machine vision. *Nat Nanotechnol*, doi: 10.1038/s41565-023-01557-2 (2024).
100. W. Xin, W. Zhong, Y. Shi, Y. Shi, J. Jing, T. Xu, J. Guo, W. Liu, Y. Li, Z. Liang, X. Xin, J. Cheng, W. Hu, H. Xu, Y. Liu, Low-Dimensional-Materials-Based Photodetectors for Next-Generation Polarized Detection and Imaging. *Advanced Materials* **36**, 2306772 (2024).
101. M. Chai, Y. Wang, C. Chen, Z. Zhao, M. Jin, T. He, Metamaterials-Based Photoelectric Conversion: From Microwave to Optical Range. *Laser Photon Rev* **16**, 2100458 (2022).
102. D. N. Neshev, A. E. Miroshnichenko, Enabling smart vision with metasurfaces. *Nat Photonics* **17**, 26–35 (2023).
103. N. Lee, M. Xue, J. Hong, J. van de Groep, M. L. Brongersma, Multi-Resonant Mie Resonator Arrays for Broadband Light Trapping in Ultrathin c-Si Solar Cells. *Advanced Materials* **35**, 2210941 (2023).
104. M. A. Green, The path to 25% silicon solar cell efficiency: history of silicon cell evolution. *Progress in Photovoltaics: Research and Applications* **17**, 183–189 (2009).
105. M. O. Reese, S. Glynn, M. D. Kempe, D. L. McGott, M. S. Dabney, T. M. Barnes, S. Booth, D. Feldman, N. M. Haegel, Increasing markets and decreasing package weight for high-specific-power photovoltaics. *Nat Energy* **3**, 1002–1012 (2018).
106. H. A. Atwater, A. Polman, Plasmonics for improved photovoltaic devices. *Nat Mater* **9**, 205–13 (2010).
107. S. K. Cushing, N. Wu, Progress and Perspectives of Plasmon-Enhanced Solar Energy Conversion. *J Phys Chem Lett* **7**, 666–675 (2016).
108. D. Derkacs, S. H. Lim, P. Matheu, W. Mar, E. T. Yu, Improved performance of amorphous silicon solar cells via scattering from surface plasmon polaritons in nearby metallic nanoparticles. *Appl Phys Lett* **89**, 20–23 (2006).
109. V. E. Ferry, A. Polman, H. A. Atwater, Light trapping in plasmonic solar cells. *Opt Express* **18**, A237–A245 (2010).
110. S. Pillai, K. R. Catchpole, T. Trupke, M. A. Green, Surface plasmon enhanced silicon solar cells. *J Appl Phys* **101**, 0–8 (2007).
111. P. Spinelli, M. A. Verschuuren, A. Polman, Broadband omnidirectional antireflection coating based on subwavelength surface Mie resonators. *Nat Commun* **3**, 692 (2012).
112. E. F. Pecora, A. Cordaro, P. G. Kik, M. L. Brongersma, Broadband Antireflection Coatings Employing Multiresonant Dielectric Metasurfaces. *ACS Photonics* **5**, 4456–4462 (2018).
113. Z. Y. Wang, R. J. Zhang, S. Y. Wang, M. Lu, X. Chen, Y. X. Zheng, L. Y. Chen, Z. Ye, C. Z. Wang, K. M. Ho, Broadband optical absorption by tunable Mie resonances in silicon nanocone arrays. *Sci Rep* **5**, 7810 (2015).
114. D. Visser, D. Y. Chen, Y. Désières, A. P. Ravishankar, S. Anand, Embossed Mie resonator arrays composed of compacted TiO2 nanoparticles for broadband anti-reflection in solar cells. *Sci Rep* **10**, 12527 (2020).
115. P. Spinelli, A. Polman, Light Trapping in Thin Crystalline Si Solar Cells Using Surface Mie Scatterers. *IEEE J. Photovoltaics* **4**, 1–6 (2014).
116. I.-K. Ding, J. Zhu, W. Cai, S.-J. Moon, N. Cai, P. Wang, S. M. Zakeeruddin, M. Grätzel, M. L. Brongersma, Y. Cui, M. D. McGehee, Plasmonic Dye-Sensitized Solar Cells. *Adv Energy Mater* **1**, 52–57 (2011).
117. N. Kooy, K. Mohamed, L. T. Pin, O. S. Guan, A review of roll-to-roll nanoimprint lithography. *Nanoscale Res Lett* **9**, 320 (2014).

118. S. H. Ahn, L. J. Guo, High-Speed Roll-to-Roll Nanoimprint Lithography on Flexible Plastic Substrates. *Advanced Materials* **20**, 2044–2049 (2008).
119. M. Leitgeb, D. Nees, S. Ruttloff, U. Palfinger, J. Götz, R. Liska, M. R. Belegratis, B. Stadlober, Multilength Scale Patterning of Functional Layers by Roll-to-Roll Ultraviolet-Light-Assisted Nanoimprint Lithography. *ACS Nano* **10**, 4926–4941 (2016).
120. J. Kim, J. Seong, W. Kim, G.-Y. Lee, S. Kim, H. Kim, S.-W. Moon, D. K. Oh, Y. Yang, J. Park, J. Jang, Y. Kim, M. Jeong, C. Park, H. Choi, G. Jeon, K. Lee, D. H. Yoon, N. Park, B. Lee, H. Lee, J. Rho, Scalable manufacturing of high-index atomic layer–polymer hybrid metasurfaces for metaphotonics in the visible. *Nat Mater* **22**, 474–481 (2023).
121. C.-L. Wu, C.-K. Sung, P.-H. Yao, C.-H. Chen, Sub-15 nm linewidth gratings using roll-to-roll nanoimprinting and plasma trimming to fabricate flexible wire-grid polarizers with low colour shift. *Nanotechnology* **24**, 265301 (2013).
122. https://www.forbes.com/sites/sabbirrangwala/2023/07/05/metalenz-pioneers-high-volume-semiconductor-foundry-based-lens-manufacturing/?sh=1577001b23bd.
123. A. Cordaro, J. Van De Groep, S. Raza, E. F. Pecora, F. Priolo, M. L. Brongersma, Antireflection High-Index Metasurfaces Combining Mie and Fabry-Pérot Resonances. *ACS Photonics* **6**, 453–459 (2019).
124. S. A. Schulz, Rupert. F. Oulton, M. Kenney, A. Alù, I. Staude, A. Bashiri, Z. Fedorova, R. Kolkowski, A. F. Koenderink, X. Xiao, J. Yang, W. J. Peveler, A. W. Clark, G. Perrakis, A. C. Tasolamprou, M. Kafesaki, A. Zaleska, W. Dickson, D. Richards, A. Zayats, H. Ren, Y. Kivshar, S. Maier, X. Chen, M. A. Ansari, Y. Gan, A. Alexeev, T. F. Krauss, A. Di Falco, S. D. Gennaro, T. Santiago-Cruz, I. Brener, M. V. Chekhova, R.-M. Ma, V. V. Vogler-Neuling, H. C. Weigand, Ü.-L. Talts, I. Occhiodori, R. Grange, M. Rahmani, L. Xu, S. M. Kamali, E. Arababi, A. Faraon, A. C. Harwood, S. Vezzoli, R. Sapienza, P. Lalanne, A. Dmitriev, C. Rockstuhl, A. Sprafke, K. Vynck, J. Upham, M. Z. Alam, I. De Leon, R. W. Boyd, W. J. Padilla, J. M. Malof, A. Jana, Z. Yang, R. Colom, Q. Song, P. Genevet, K. Achouri, A. B. Evlyukhin, U. Lemmer, I. Fernandez-Corbaton, Roadmap on photonic metasurfaces. *Appl Phys Lett* **124** (2024).
125. E. Khaidarov, D. Eschimese, K. H. Lai, A. Huang, Y. H. Fu, Q. Lin, R. Paniagua-Dominguez, A. I. Kuznetsov, Large-scale vivid metasurface color printing using advanced 12-in. immersion photolithography. *Sci Rep* **12**, 14044 (2022).
126. N. Li, Z. Xu, Y. Dong, T. Hu, Q. Zhong, Y. H. Fu, S. Zhu, N. Singh, Large-area metasurface on CMOS-compatible fabrication platform: driving flat optics from lab to fab. *Nanophotonics* **9**, 3071–3087 (2020).
127. C. Park, W. Kim, Y. Kim, H. Sung, J. Park, H. Song, J. Kim, D. K. Oh, H. Kang, N. Jeon, J. Rho, H. Lee, High-Throughput Fabrication of Large-Scale Metaholograms via One-step Printing. *Adv Opt Mater* **12** (2024).

Acknowledgments:

Funding:

S.T.H, J.K.W.Y, H.V.D and A.I.K acknowledge the funding support from Singapore MTC-Programmatic grant No: M21J9b0085.

J.K.W.Y also acknowledges support from Singapore NRF Investigatorship Award grant No: NRF-NRFI06-2020-0005.

H.V.D also acknowledges support from TÜBA-Turkish Academy of Sciences.

Q.L. and M.L.B. acknowledge funding from an AFOSR MURI grant (No. FA9550-17-1-0002) and the US Department of Energy grant (No. DE-FG07-ER46426).

Competing interests: Authors declare that they have no competing interests.